



## Research Article

<https://doi.org/10.1631/jzus.A2400271>

# Study on the co-removal potential of heavy metals and dyes from wastewater by simultaneous adsorption with biomass residue formed from microbial treatment of lacquer residue

Xinyue LU<sup>1</sup>, Min LIAO<sup>1</sup>✉, Xiaomei XIE<sup>2</sup>✉, Hao QIU<sup>1</sup>, Feng YUAN<sup>1</sup>, Zhe LUO<sup>1</sup>, Chunlin FAN<sup>3</sup>

<sup>1</sup>Zhejiang Key Laboratory of Agricultural Resources and Environment, College of Environmental and Resource Science, Zhejiang University, Hangzhou 310058, China

<sup>2</sup>Experimental Teaching Center, College of Environmental and Resource Science, Zhejiang University, Hangzhou 310058, China

<sup>3</sup>Ningbo Ferno Biotechnology Co., Ltd, Ningbo 315502, China

**Abstract:** This study aims to optimize the uses of lacquer residue biomass (LBM). We investigated the ability of LBM to remove Pb<sup>2+</sup> heavy metal ions and the typical cationic dye methylene blue (MB) and anionic dye Congo red (CR) by simultaneous adsorption from composite systems, as well as the relevant factors. Scanning electron microscopy (SEM), X-ray diffraction (XRD), and Fourier transform infrared spectroscopy (FTIR) were used to characterize adsorption behavior. The adsorption kinetics of Pb<sup>2+</sup>-MB/CR composite systems can be effectively characterized by the pseudo-second-order kinetic model ( $R^2 > 0.99$ ). In the Pb<sup>2+</sup>-MB composite system, adsorption was antagonistic with similar adsorption sites. However, in the Pb<sup>2+</sup>-CR composite system, we found that adsorption was synergistic with different adsorption sites, which led to a higher simultaneous adsorption capacity for a higher initial Pb<sup>2+</sup>-CR concentration, unlike the Pb<sup>2+</sup>-MB system. In both composite systems, an appropriate increase in LBM dosage and system temperature within a certain range was conducive to simultaneous adsorption and removal of Pb<sup>2+</sup>-MB/CR composite systems. The optimal solid-liquid ratio and temperature were 1:75 and 30 °C. The adsorption and removal rates of Pb<sup>2+</sup> and MB were 99.98% and 90.49%, respectively, and those of Pb<sup>2+</sup> and CR were 93.99% and 77.39%, respectively, in (50, 50) mg/L of Pb<sup>2+</sup>-MB/CR composite systems under these conditions. Adsorption removal of Pb<sup>2+</sup> and MB improved with higher pH levels, and worsened with the increase of ionic strength in the solution, while the removal rate of CR showed an opposite trend. The coexisting anion and cation types had limited influence on the simultaneous adsorption removal of Pb<sup>2+</sup>, MB, and CR. The results of desorption showed that LBM can be utilized as a disposable material for simultaneously treating Pb<sup>2+</sup>-MB/CR composite systems. The simultaneous adsorption mechanisms of Pb<sup>2+</sup>-MB/CR mainly involved hydrogen bonding,  $\pi$ - $\pi$  bonding interaction, and electrostatic interaction.

**Key words:** Lacquer residue biomass; Lead; Methylene blue; Congo red; Simultaneous adsorption removal

## 1 Introduction

With the ongoing urbanization and industrialization in China, large quantities of wastewater are continuously released into the aquatic ecosystem, including organic and inorganic pollutants, pesticides, heavy metals, and dyes. Because dyeing and printing are major industries in the country, the

wastewater from the Chinese textile-dyeing and printing sector constitute a significant proportion (approximately 40%) of the overall volume of industrial wastewater released. Synthetic dyes are the main pollutants (Cai, 2018; Lin et al., 2023; Ye et al., 2020a; Ye et al., 2020b; Ye et al., 2024). Due to their unique chemical properties, they possess characteristics such as a wide range of pollutants, long duration, and resistance to biodegradation. Cr, Pb, Cu, Ni, Fe, Zn, Hg, Cd and other heavy metal elements remain in wastewater as well. Catalysts, mordants, and metal antimicrobial additives are all sources of these heavy metals (Song et al., 2023; Cang et al., 2021; Li et al., 2019b). Most heavy metals, dyes, and dye metabolites accumulate in large quantities in animals,

✉ Min LIAO, liaomin@zju.edu.cn

Xiaomei XIE, xiexiaomei@zju.edu.cn

Min LIAO, <https://orcid.org/0000-0001-9078-204X>

Received May 24, 2024; Revision accepted Aug. 4, 2024;  
Crosschecked

humans, and the environment, which can cause extensive damage to humans and ecosystems even at low concentrations. In the past, treatment of such compound polluted wastewater was often characterized by a combination of several methods, which was cumbersome and costly. Therefore, it is critical to reasonably design and develop a single material for the simultaneous removal of compound pollutants.

Current methods for removing heavy metals and dyes from wastewater include chemical precipitation, ion exchange, photocatalytic degradation, advanced oxidation processes, and adsorption; or combinations of these techniques (Kim et al., 2021; Li et al., 2022; Ma et al., 2021). Adsorption technology is widely used because of its high efficiency, low cost, easy operation, energy savings, and sustainability (Alorabi and Azizi, 2023). At present, biomass materials from various byproducts and wastes left by industrial, agricultural, and forestry production are seen as potential adsorption materials because of their economic accessibility and sustainability. The surface of these byproducts has a porous structure, and contains rich active functional groups such as aminos, carboxyls, and hydroxyls, and organic matter such as cellulose, amino acids, lipids, and other substances that have strong interactions with anionic, cationic dyes, and heavy metals, respectively. This results in excellent adsorption properties with regard to heavy metals and dyes. Many biomass materials have been used in composite pollution systems with heavy metals and dyes, such as cellulose materials, bagasse, fruit peel, humus, and solid-waste ash (An et al., 2023; Meneses et al., 2022; Chen et al., 2024b; Xie et al., 2020). Cyclic venturi bioreactor technology is the latest microbial treatment process developed by our research group, which has been applied in a series of equipment enterprises including Yanfeng Automotive Decoration System Wuhan Co., Ltd of China. The lacquer components are fully degraded in operation, however this leaves biomass (LBM) that contains more nascent organic matter and virgin mineral fillers that are also rich in functional groups. If LBM can be used, this would not only avoid the risks caused by improper disposal of waste, but also meet the "Carbon Peaking and Carbon Neutrality Goals," which offers economic value. LBM has been re-

ported to be a better adsorbent for anionic and cationic dyes in single systems (Lu et al., 2024), but it remains to be investigated whether LBM could serve as an innovative adsorbent for managing wastewater contaminated with both dyes and heavy metals.

In view of this, we used LBM as our research object, and selected the heavy metal  $\text{Pb}^{2+}$ , the cationic dye MB, and the anionic dye CR as the target pollutants to construct simulated composite wastewater systems. We then explored the simultaneous removal ability for  $\text{Pb}^{2+}$ -MB/CR composite systems as well as the interactions between  $\text{Pb}^{2+}$  and MB or CR.

This approach revealed the application potential of LBM, with a view to offering an affordable, readily accessible, and ecological biomass material for concurrent remediation of heavy metals and dyes in wastewater, and also using a "waste resource".

## 2 Materials and methods

### 2.1 Reagents and Instruments

Chemical reagents: MB, CR,  $\text{Pb}(\text{NO}_3)_2$ ,  $\text{H}_2\text{SO}_4$ ,  $\text{HNO}_3$ , HCl, NaCl were analytically pure and purchased from Sinopharm Chemical Reagent Co. The structural formulas of MB and CR are shown in Appendix A Fig. S1.

Instruments: electronic analytical balance (BSA224S-CW, Sartorius, Germany), UV spectrophotometer (UV-2450, Shimadzu, Japan), pH meter (PHS-25, Shanghai Yidian Co., Ltd., China), thermostatic oscillator (HZ-9211KB, Jiangsu Taicang Science and Education Equipment Factory, China), benchtop low-temperature centrifuge (L-550, Hunan Xiang Yi Laboratory Instrument Development Co., Ltd., China), Atomic Absorption Spectrometer (NOVAA300, Jena Analytical Instruments AG, Germany), scanning electron microscope (SU8010, Hitachi Scientific Instruments Ltd., China), X-ray diffractometer (Bruker D8 Advance, Bruker Ltd., Germany), Fourier infrared spectroscopy (NICOLET iS50FT-IR, Thermo Fisher, USA).

### 2.2 Source and preparation of LBM

The LBM used here was from the recirculating venturi bioreactor in the microbial treatment section for residual spray lacquer mist in Yanfeng Auto-

tive Decoration System Wuhan Co., Ltd. The treatment of this bioreactor was carried out by bacterial strains including the strain group *Beijerinckia sp.* with adhesive and dispersing properties (LM-W, preservation number: CGMCC No.17168), *Brachymonas sp.* with flocculation and precipitation properties (LM-R, preservation number: CGMCC No.17167) (patented by our research group), and the residual product obtained after treatment was dried to produce the LBM biomass used in this experiment, which had a moisture content of 1.00%. Additionally, the dried LBM was sifted through a 100-mesh sieve. The obtained LBM consisted mainly of organic matter (56.24% organic matter and 29.75% protein). Of the major constituent elements, C had the highest mass fraction of 36.79%. There were many mineral fillers from the original lacquer in the LBM; the content of  $\text{CaCO}_3$ ,  $\text{SiO}_2$ ,  $\text{TiO}_2$ ,  $\text{Fe}_2\text{Ti}_3\text{O}_9$ , and  $\text{Ca}_3(\text{PO}_4)_2$  was 34.75%, 0.19%, 5.19%, 1.07%, and 0.78%, respectively. Meanwhile, no content of harmful heavy metals such as Pb, Cd Zn, Cr, Cu, was detected, and extractable forms of the above elements in the leachate and dissolved organics were not detected either. Therefore the LBM could be classified as a material with lower environmental risk. The surface of the LBM was predominantly negatively charged ( $\text{pH}_{\text{pzc}}$  was about 4.10), and exhibited relatively moderate pore size, specific surface area, and pore volume. It also had good water permeability, which showed its promise as an adsorbent. Detailed measurements and data sources for the above basic physical and chemical properties of LBM are available in the published literature (Lu et al., 2024).

### 2.3 Adsorption kinetics of the $\text{Pb}^{2+}$ -MB/CR composite systems

LBM was weighed into a series of 50 mL centrifuge tubes (0.20 g per tube), and 15 mL (50, 50) mg/L of  $\text{Pb}^{2+}$ -MB/CR composite systems solutions (pH 5.0) was added for adsorption reaction in the thermostatic oscillator at 180 r/min and 30 °C. Samples were taken from the centrifuge tubes at different adsorption-reaction times, and the supernatant was obtained after centrifugation at a speed of 4000 r/min for 10 min. The concentration of  $\text{Pb}^{2+}$ , MB, or CR in the supernatant was determined by Atomic Absorp-

tion Spectrometer or UV spectrophotometer (Azeez et al., 2022; Mu et al., 2022; Wang et al., 2024b). We used the pseudo-first-order kinetic model (Eq. (1)) and pseudo-second-order kinetic model (Eq. (2)) to fit the adsorption data.

$$\ln(q_e - q_t) = \ln q_e - k_1 t \quad (1)$$

$$\frac{t}{q_t} = \frac{1}{k_2 q_e^2} + \frac{t}{q_e} \quad (2)$$

where  $q_e$  is the adsorption capacity at equilibrium (mg/g);  $q_t$  is the adsorption capacity at different moments (mg/g); and  $K_1, K_2$  are the kinetic rate constants (mg/g).

### 2.4 Isothermal adsorption of the $\text{Pb}^{2+}$ -MB/CR composite systems

LBM was weighed into a series of 50 mL centrifuge tubes (0.20 g per tube), and 15 mL different initial concentrations of  $\text{Pb}^{2+}$ -MB/CR composite systems solution (pH 5.0) was added for adsorption reaction in the thermostatic oscillator at 180 r/min and 30 °C. When the adsorption reached equilibrium, the supernatant was obtained after centrifugation at a speed of 4000 r/min for 10 min, and the concentration of  $\text{Pb}^{2+}$ , MB or CR in the supernatant was determined. Langmuir (Eq. (3)) and Freundlich (Eq. (4)) isothermal adsorption models were fitted linearly.

$$\frac{1}{q_e} = \frac{1}{q_{\max} K_L} + \frac{C_e}{q_{\max}} \quad (3)$$

$$\ln q_e = \frac{1}{n} \ln C_e + \ln K_F \quad (4)$$

$$R_L = \frac{1}{1 + K_L C_0} \quad (5)$$

where  $q_e$  is the adsorption capacity at equilibrium (mg/g);  $C_e$  is the equilibrium concentration (mg/L);  $q_{\max}$  is the maximum adsorption capacity of the adsorbent;  $K_L$  is the Langmuir constant (L/mg);  $K_F$  ((mg/g) (L/mg)<sup>1/n</sup>),  $n$  are Freundlich constants;  $C_0$  is the highest initial concentration of the adsorbate (mg/L); and  $R_L$  reflects the affinity of the adsorption process.

### 2.5 Adsorption thermodynamics of the $\text{Pb}^{2+}$ -MB/CR composite systems

To further understand the impact of temperature during adsorption in the  $\text{Pb}^{2+}$ -MB/CR composite systems, Eqs. (6) (7) (8) serve to calculate the ther-

thermodynamic parameters of the two composite systems, including the Gibbs free energy ( $\Delta G^\circ$ ), enthalpy ( $\Delta H^\circ$ ), and entropy ( $\Delta S^\circ$ ) (Shubham and Jyoti, 2024).

$$K = \frac{C_{ad,e}}{C_e} \quad (6)$$

$$\Delta G^\circ = \Delta H^\circ - T\Delta S^\circ \quad (7)$$

$$\ln K = \frac{\Delta S^\circ}{R} - \frac{\Delta H^\circ}{RT} \quad (8)$$

Eq. (5) defines the standard thermodynamic equilibrium constant  $K$  (Han et al., 2009).  $C_{ad,e}$  is the concentration of adsorbate on the adsorbent at equilibrium.  $C_e$  is the equilibrium concentration (mg/L).  $\Delta G^\circ$  is the Gibbs free energy (kJ/mol);  $\Delta H^\circ$  is the enthalpy (kJ/mol);  $\Delta S^\circ$  is the entropy (kJ/(mol K));  $R$  is the universal gas constant (8.314 J/(mol K)); and  $T$  is the reaction temperature (K).

## 2.6 Influence of system adsorption conditions

We investigated the effect of different adsorption conditions on the adsorption performance of the  $Pb^{2+}$ -MB/CR systems ((50, 50) mg/L) with regard to pH (1.0-5.0), background NaCl ionic strength (0.01-0.05 mol/L), LBM dosage (0.05-0.40 g), and adsorption temperature (10-50 °C), based on the monofactor analysis. We then carried out the adsorption reactions in the thermostatic oscillator at 180 r/min. When adsorption reached equilibrium, the supernatant was obtained after centrifugation at a speed of 4000 r/min for 10 min, and the concentration of  $Pb^{2+}$ , MB, or CR in the supernatant was determined. The relationship between solid-liquid ratio and dosage is shown in Appendix A Table S1.

## 2.7 Interactions between coexisting pollutants in the composite systems

To explore the interactions between  $Pb^{2+}$  and MB or CR in the composite systems, we set the following concentration combinations (see Appendix A Table S2). 15 mL of the composite wastewater described above was added to 50 mL centrifuge tubes containing 0.05g of LBM, and adsorption reaction conditions were the same as described. The supernatant was obtained after centrifugation at a speed of 4000 r/min for 10 min when adsorption reached equilibrium, and the concentrations of  $Pb^{2+}$ , MB, or

CR in the supernatant were determined. The interaction was evaluated with the ratio of adsorption capacity  $R_{q,i}$  (Eq. (9)) (Du et al., 2022).

$$R_{q,i} = \frac{q_{m,i}}{q_{s,i}} \quad (9)$$

where  $R_{q,i}$  is the ratio of the adsorption capacity, which is usually categorized into three types: synergistic effect ( $R_{q,i} > 1$ ), indicating a promotional effect within the system; no interaction ( $R_{q,i} = 1$ ), signifying no effect; and antagonistic effect ( $R_{q,i} < 1$ ), denoting an inhibitory effect. The adsorption capacity (mg/g) of adsorbate  $i$  ( $Pb^{2+}$ , MB, or CR) in single or composite systems under the same adsorption conditions is denoted by  $q_{s,i}$  and  $q_{m,i}$  respectively.

## 2.8 Effect of coexisting anions and cations on adsorption of LBM in the $Pb^{2+}$ -MB/CR composite systems

LBM was weighed into a series of 50 mL centrifuge tubes (0.20 g per tube), and 15 mL (50, 50) mg/L  $Pb^{2+}$ -MB/CR composite solution was added containing  $Na^+$ ,  $Mg^{2+}$ , and  $Ca^{2+}$  cations (in the form of chloride salt), and  $CO_3^{2-}$ ,  $SO_4^{2-}$ , and  $PO_4^{3-}$  anions (in the form of sodium salt) (pH 5.0), with a resulting ionic strength of 0.03 mol/L. The adsorption reactions were carried out in the composite systems in the thermostatic oscillator at 180 r/min and 30 °C. The supernatant was obtained after centrifugation at 4000 r/min for 10 min when adsorption reached equilibrium. Finally, the concentration of  $Pb^{2+}$  and MB or CR in the supernatant was determined.

## 2.9 Calculation of adsorption capacity and adsorption removal rate

The adsorption capacity  $q$  (Eq. (10)) and removal rate  $\eta$  (Eq. (11)) can be used to express the effect of adsorption.

$$q = \frac{(C_0 - C_e) \cdot V}{W} \quad (10)$$

$$\eta = \frac{(C_0 - C_e)}{C_0} \times 100\% \quad (11)$$

where  $q$  is the adsorption capacity at equilibrium (mg/g);  $C_0$  is the initial concentration of the adsorbate (mg/L);  $C_e$  is the equilibrium concentration (mg/L);  $V$  is the volume of the adsorbent solution (L); and  $W$  is the dosage of LBM (g).

## 2.10 Desorption of LBM

LBM was weighed into a series of 50 mL centrifuge tubes (0.20 g per tube), and 15 mL (50, 50) mg/L  $\text{Pb}^{2+}$ -MB/CR composite solution (pH 5.0) was added. The adsorption reactions in the composite systems were carried out in the thermostatic oscillator at 180 r/min and 30 °C. The concentrations of  $\text{Pb}^{2+}$  and MB or CR in the supernatant were determined when the adsorption reached equilibrium. We separated the adsorbed-state LBM from the composite systems and obtained the residual liquid volume  $V_0$  by the gravimetric method. Subsequently, 15 mL of 0.1 mol/L  $\text{H}_2\text{SO}_4$ , 0.1 mol/L  $\text{HNO}_3$ , and 0.1 mol/L  $\text{HCl}$  were used as desorbents. The desorption reactions were carried out in a thermostatic oscillator at 180 r/min and 30 °C. After desorption reached equilibrium, the supernatant was obtained after centrifugation at a speed of 4000 r/min for 10 min. The concentration of  $\text{Pb}^{2+}$ , MB or CR in the supernatant was determined, and the desorption capacity  $\lambda$  (Eq. (12)) and desorption rate  $\theta$  (Eq. (13)) were calculated.

$$\lambda = C_t(V_t + V_0) - C_e V_0 \quad (12)$$

$$\theta = \frac{\lambda}{q} \times 100\% \quad (13)$$

where  $C_t$  is the concentration of desorbed adsorbate (mg/L);  $C_e$  is the equilibrium concentration (mg/L);  $V_t$  is the desorbed liquid volume (L); and  $V_0$  is the residual liquid volume (L).

## 2.11 Characterization of adsorption behavior

We observed and analyzed the LBM before and after adsorption with SEM, XRD, and FTIR. The surface morphology characteristics were observed with SEM at an accelerating voltage of 3 kV. The FTIR with the potassium bromide pressurizations method controlled by the frequency range of 4000-400  $\text{cm}^{-1}$  with a spectral resolution of 4  $\text{cm}^{-1}$  and 32 scans for samples. The XRD measurement conditions were as follows: copper k-alpha, with a tube current and scanning range of 40 mA and 5-90 °, respectively.

## 3 Results and discussion

### 3.1 Kinetic characterization of adsorption in $\text{Pb}^{2+}$ -MB/CR composite systems

Adsorption is divided into three stages: transportation of the substance from the liquid phase to the boundary layer at the surface of the adsorbent; attachment to the surface of the adsorbent; and penetration into pore spaces. Initially, the rate of adsorption is typically rapid, and then it reaches a constant value (Igberase et al., 2018; Sepideh et al., 2024).

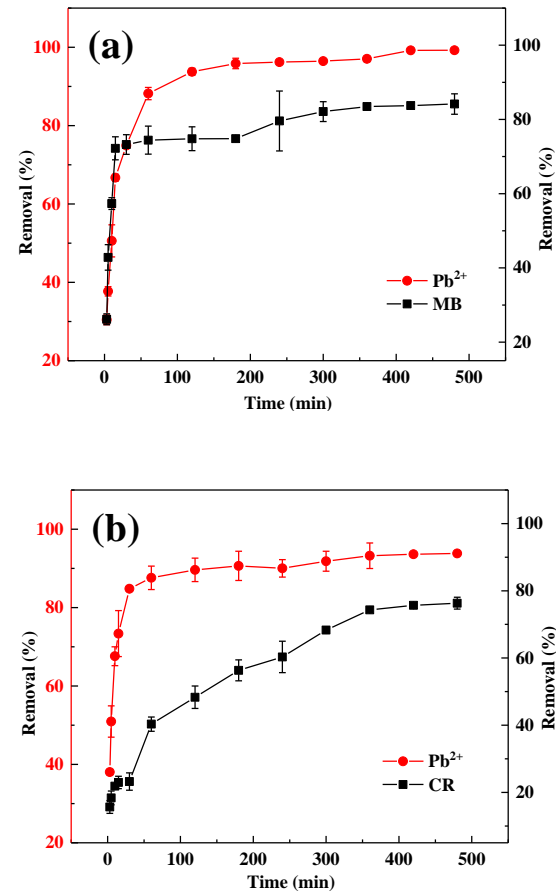


**Fig. 1** Effect of adsorption time on LBM adsorption of  $\text{Pb}^{2+}$ -MB (a) and  $\text{Pb}^{2+}$ -CR (b) composite systems

It can be observed from Fig. 1 that for the  $\text{Pb}^{2+}$ -MB system, at the onset of the adsorption process, the adsorption of  $\text{Pb}^{2+}$  from 0-60 min, of MB from 0-30 min, and the adsorption removal rate of  $\text{Pb}^{2+}$  and MB by LBM increased linearly as the fast adsorption process was extended. The adsorption removal rate of  $\text{Pb}^{2+}$  and MB within 60 min and 30 min reached 88.18% and 73.24%, respectively. The adsorption rate depends on the availability of adsorption sites (Morteza et al., 2021; Nizam et al.,

2024). Therefore, the fast adsorption rate and high removal efficiency we observed can be attributed to the large number of surface vacancies on the LBM. And the initial concentration during the early phase offered a significant impetus that facilitated the overcoming of mass transfer resistance between the aqueous phase and solid phase for the adsorbate ions (Tattibayeva et al., 2022). With longer times, we observed that the adsorption capacity continued to increase, albeit at a decelerating pace, which indicated a slow reaction process. Adsorption reactions tended to equilibrate after 300 min, and finally achieved maximum adsorption removal. The adsorption removal rates of  $\text{Pb}^{2+}$  and MB by LBM respectively reached 99.23% and 84.16%. These phenomena can be explained by adsorbate ions gradually occupying the active site of the adsorbent. The enhancement of mass transfer resistance caused by the decrease of adsorbate concentration in the solution might also slow down the adsorption process, causing the adsorption reactions to reach the adsorption equilibrium.

In the  $\text{Pb}^{2+}$ -CR system, when  $\text{Pb}^{2+}$  and CR were adsorbed for 0-30 min and 0-60 min, their adsorption removal rate increased linearly with the prolongation of time, which would also be considered a fast adsorption process. In comparison to what we saw in the  $\text{Pb}^{2+}$ -MB system, the adsorption rate of LBM for  $\text{Pb}^{2+}$  was faster. Therefore, we speculate that coexisting CR has a smaller effect on the adsorption of  $\text{Pb}^{2+}$ . Compared with MB, the adsorption of CR had a longer adsorption reaction time and relatively smaller adsorption removal rate owing to the formation of strong electrostatic attraction between the LBM (negative charge) and the MB (positive charge and cationic type), which promoted fast adsorption of MB. The removal of  $\text{Pb}^{2+}$  and CR increased slowly with longer contact time, indicating a slow reaction process, and the adsorption reactions reached equilibrium at 360 min ( $\text{Pb}^{2+}$ ) and 360 min (CR). Finally, the adsorption removal rates of  $\text{Pb}^{2+}$  and CR respectively reached 93.81% and 76.32%. It was clear that the adsorption removal rate of  $\text{Pb}^{2+}$  in the system with a lower initial concentration of  $\text{Pb}^{2+}$ -MB was slightly higher than in the  $\text{Pb}^{2+}$ -CR system, but the

adsorption removal rates of  $\text{Pb}^{2+}$  were all higher than 93% in both composite systems. These results might be due to LBM with a negatively charged surface having enough adsorption sites for  $\text{Pb}^{2+}$  at lower initial concentrations; however, more negatively charged CR was retained in solution by the negative-charge surface repulsion of LBM in the  $\text{Pb}^{2+}$ -CR system, and sulfonic acid groups on CR in solution could bind to  $\text{Pb}^{2+}$ , which slightly reduced the adsorption removal rate of  $\text{Pb}^{2+}$  in the  $\text{Pb}^{2+}$ -CR system. The structural formula of CR is shown in Appendix A Fig. S1.

To gain a deeper understanding of the kinetic properties of LBM adsorption in the  $\text{Pb}^{2+}$ -MB/CR composite systems, we applied both the pseudo-first-order and pseudo-second-order kinetic models to fit the kinetic data (the outcomes are detailed in Table 1). According to the  $R^2$  value of the fitting results, the pseudo-second-order kinetic model provided a more precise representation of the adsorption process for both systems ( $R^2 > 0.99$ ). The adsorption capacities predicted by the pseudo-second-order kinetic model for  $\text{Pb}^{2+}$  and MB were 15.08 mg/g and 3.17 mg/g, respectively, and the experimental data closely aligned with the actual figures (14.89 mg/g and 3.16 mg/g). Meanwhile the adsorption capacities predicted for  $\text{Pb}^{2+}$  and CR were 14.14 mg/g and 3.04 mg/g, respectively. The experimental data also closely aligned with the actual figures (14.07 mg/g and 2.86 mg/g), suggesting that adsorption in the  $\text{Pb}^{2+}$ -MB/CR composite systems was controlled by chemical mechanisms (Fan et al., 2018; Lv et al., 2019).

**Table 1 Kinetic parameters of the pseudo-first-order kinetic and pseudo-second-order kinetic**

Adsorbate	Concentration mg/L	Pseudo-first-order kinetic				Pseudo-second-order kinetic			
		$q_{e.exp}$ mg/g	$q_{e.cal}$ mg/g	$k_1$ $min^{-1}$	$R^2$	$q_{e.exp}$ mg/g	$q_{e.cal}$ mg/g	$k_2$ g/(mg min)	$R^2$
Pb <sup>2+</sup>	50	14.89	7.12	0.03	0.88	14.89	15.08	0.01	0.99
MB		3.16	1.06	0.02	0.88	3.16	3.17	0.04	0.99
Pb <sup>2+</sup>	50	14.07	3.40	0.01	0.69	14.07	14.14	0.01	0.99
CR		2.86	3.10	0.02	0.87	2.86	3.04	0.01	0.97

### 3.2 Isothermal adsorption in Pb<sup>2+</sup>-MB/CR composite systems

Adsorption isotherms predominantly depict the nature of interactions that occur between the adsorbate and adsorbent, and their relationship. Monolayer molecular adsorption with uniform adsorption capacity on the adsorbent surface is represented well by the Langmuir isotherm model, whereas multilayer molecular adsorption by an adsorbent with an uneven surface-active site more suited to the Freundlich isotherm model. Moreover, the energy distribution of the adsorption site decreases exponentially (Kalam et al., 2021; Nitish et al., 2023; Zhang et al., 2023b). We utilized both isothermal adsorption models to analyze the isothermal adsorption data of Pb<sup>2+</sup>-MB/CR composite systems, as depicted in Fig. 2 and Table 2.

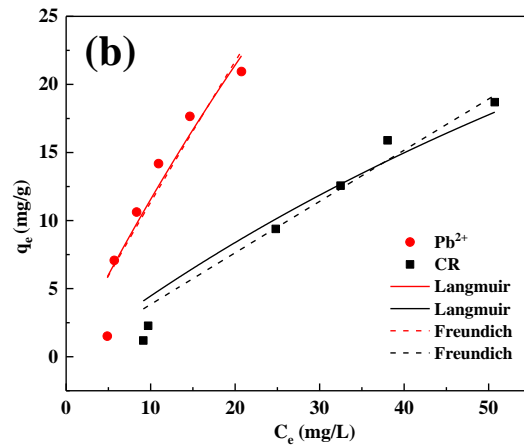
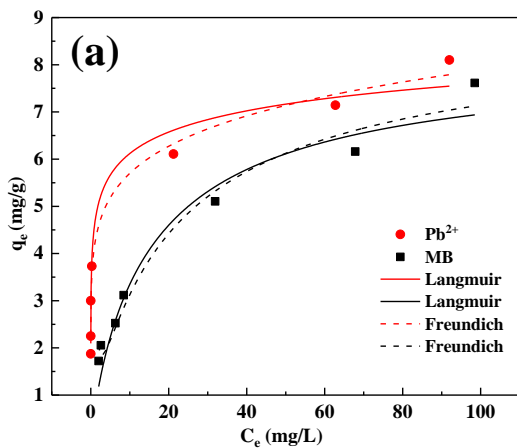


**Fig. 2 Langmuir and Freundlich adsorption isotherms of Pb<sup>2+</sup>-MB (a) and Pb<sup>2+</sup>-CR (b) composite systems**

It can be seen from Fig. 2 and Table 2 that the Langmuir isotherm adsorption model only better characterizes isothermal adsorption by LBM in the Pb<sup>2+</sup>-MB composite system ( $R^2 > 0.97$ ). It exemplifies the intricate nature of adsorption of Pb<sup>2+</sup>/MB on LBM, arising from diverse chemical interactions such as chemical bonding between adsorbate ions and adsorbent surfaces, and electrostatic forces between adsorbate ions and surface functional groups. The maximum adsorption capacity for Pb<sup>2+</sup> and MB was 7.63 mg/g and 7.98 mg/g, respectively, at 30 °C.  $R_L$  is a non-dimensional equilibrium parameter representing the equilibrium adsorption behavior, which can reflect whether the adsorption process is irreversible ( $R_L = 0$ ), favorable ( $0 < R_L < 1$ ), linear ( $R_L = 1$ ), or unfavorable ( $R_L > 1$ ). The results of  $R_L$  revealed that adsorption of Pb<sup>2+</sup> and MB was a favorable adsorption process on LBM, and Pb<sup>2+</sup> and MB had a high affinity with the LBM (Table 2). But, the Freundlich isothermal adsorption model had better fitting results for Pb<sup>2+</sup>-MB ( $R^2 > 0.95$ ) or Pb<sup>2+</sup>-CR ( $R^2 > 0.90$ ) composite systems simultaneously adsorbed by LBM. This

model accounts for multilayer adsorption, in which the heat of adsorption and affinity are not uniformly distributed on a non-homogeneous surface (Hajiahmadi et al., 2024). The intensity of the interactions between the adsorbate and adsorbent can be inferred from the surface heterogeneity factor  $1/n$ . If  $1/n$  tends towards 0, this indicates that it might be more heterogeneous in nature; if it is between  $0 < 1/n < 1$ , this signifies that the level of adsorption is favorable. If  $1/n=1$ , it implies that adsorption is independent of the concentration of the adsorbent. Conversely, if  $1/n > 1$ ,

adsorption is unfavorable and the affinity is weak (Alorabi and Azizi, 2023; Debnath and Das, 2023; Mondal et al., 2024). We found that the  $1/n$  value was less than 1 for  $Pb^{2+}$ -MB/CR composite systems, which suggests that the adsorption processes in  $Pb^{2+}$ -MB/CR were effective and that the complex multi-layer adsorption processes were dominated by chemisorption (see Selim et al., 2024). The above results show that the adsorption performance of LBM for different composite systems of  $Pb^{2+}$ -MB/CR might be controlled by different mechanisms.

**Table 2 Parameters of Langmuir and Freundlich isothermal adsorption models**

Adsorbate	$q_{e.exp}$ mg/g	Langmuir isothermal adsorption model				Freundlich isothermal adsorption model		
		$q_{max}$ mg/g	$K_L$ L/mg	$R_L$	$R^2$	$K_F$ (mg/g) (L/mg) <sup>1/n</sup>	$1/n$	$R^2$
$Pb^{2+}$	8.10	7.63	0.60	0.01	0.98	4.17	0.13	0.95
MB	7.61	7.98	0.08	0.05	0.97	1.37	0.37	0.99
$Pb^{2+}$	14.18	68.30	0.02	0.21	0.89	1.32	0.94	0.90
CR	12.56	86.66	0.01	0.48	0.88	0.39	0.99	0.96

### 3.3 Thermodynamics of the $Pb^{2+}$ -MB/CR composite systems

The adsorption thermodynamic parameters of the  $Pb^{2+}$ -MB/CR composite systems at different temperatures are shown in Table 3-4. The  $\Delta G^\circ$  of  $Pb^{2+}$ , MB, and CR in both systems was negative, which confirmed that the adsorption had good spontaneity (I.M.S. et al., 2023). Meanwhile, the  $\Delta G^\circ$  increased when temperature rose, which showed that the spontaneity of the process was enhanced. This means that a higher temperature favors adsorption in both systems.  $\Delta H^\circ$  was positive, which further proved that adsorption of  $Pb^{2+}$ , MB and CR by LBM was endothermic. In addition, the positive  $\Delta S^\circ$  denoted an increase in the level of stoichiometry at the solid-liquid interfaces in the systems (Angaru et al., 2021; Vikram et al., 2024).

**Table 3 Thermodynamic parameters of the  $Pb^{2+}$ -MB composite system**

Adsorbate	Temperature K	$\Delta G^\circ$ kJ/mol	$\Delta H^\circ$ kJ/mol	$\Delta S^\circ$ kJ/(mol K)
$Pb^{2+}$	293	-12.37	8.39	0.07
	303	-13.08		

MB	313	-13.79	57.94	0.20
	293	-0.93		
	303	-2.94		
	313	-4.95		

**Table 4 Thermodynamic parameters of the  $Pb^{2+}$ -CR composite system**

Adsorbate	Temperature K	$\Delta G^\circ$ kJ/mol	$\Delta H^\circ$ kJ/mol	$\Delta S^\circ$ kJ/(mol K)
$Pb^{2+}$	293	-3.02	64.15	0.23
	303	-5.32		
	313	-7.61		
CR	293	-1.17	32.89	0.12
	303	-2.33		
	313	-3.49		

### 3.4 Influence of system adsorption conditions

#### 3.4.1 Dosage of LBM

Appendix A Fig. S2 shows the comparison of adsorption in  $Pb^{2+}$ -MB (a) and  $Pb^{2+}$ -CR (b) composite systems with different LBM dosage. It is clear from the figure that adsorption and removal of  $Pb^{2+}$ , MB, and CR rose as the dosage increased, with the amount of adsorbent exerting a stronger effect on adsorption



of MB and CR.

For the  $\text{Pb}^{2+}$ -MB system, the adsorption removal rate of  $\text{Pb}^{2+}$  gradually rose from 96.94% to 99.98% when the dosage went from 0.05 g to 0.40 g. With a dosage change from 0.20 g to 0.40 g, the adsorption removal rate increased slowly, by only 0.52%. For MB, when the dosage was 0.40 g, the adsorption removal rate for the different concentrations reached the maximum, rising from 51.80% to 90.49%. This was a result of the significant increase of surface area in contact with LBM and the usability of LBM adsorption sites (Abbasi et al., 2024). While the adsorption capacity of both decreased,  $\text{Pb}^{2+}$  decreased from 14.54 mg/g to 1.87 mg/g and MB decreased from 7.77 mg/g to 1.70 mg/g. An explanation for this tendency is that the number of active adsorption sites increased when the dosage of adsorbent increased; however, due to the limited adsorbate concentration, the utilization efficiency of these sites was reduced, leading to a decrease in the mass per unit adsorption capacity of LBM (Yang et al., 2023).

For the  $\text{Pb}^{2+}$ -CR system, when the dosage changed from 0.05 g to 0.40 g, the adsorption removal rate of  $\text{Pb}^{2+}$  increased from 90.15% to 93.99%. For CR, when the dosage changed from 0.05 g to 0.40 g, the adsorption removal rate increased from 65.55% to 77.39%. When the dosage changed from 0.20 g to 0.40 g, adsorptive removal of  $\text{Pb}^{2+}$  and CR tended to flatten out. In addition, the adsorption capacity for both  $\text{Pb}^{2+}$  and CR decreased, from 13.52 mg/g to 1.76 mg/g and 9.83 mg/g to 1.45 mg/g, respectively. Although a high dosage achieved the best adsorption removal rate, saturation of the active site and avoidance of excessive waste were the keys to obtaining the best economic benefit. Adsorption removal of both  $\text{Pb}^{2+}$  and CR in the composite systems had good performance when the dosage was 0.20 g, so for the rest of the study, we determined a solid-liquid ratio of 1:75 to be the best adsorbent dosage.

### 3.4.2 System pH

The pH of a solution affects the chemical form of metals and the protonation or deprotonation of adsorbates and adsorbents; Therefore pH is a important factor during adsorption (Wang et al., 2019). Taking into consideration the hydroxide precipitation be-

havior of  $\text{Pb}^{2+}$  under alkaline conditions, we carried out the adsorption experiments in the  $\text{Pb}^{2+}$ -MB/CR composite systems at a pH of 1.0-5.0.

Appendix A Fig. S3 shows that the adsorption removal rate and adsorption capacity of  $\text{Pb}^{2+}$  and MB in the  $\text{Pb}^{2+}$ -MB composite system increased with the increase of pH. After the pH increased from 1.0 to 5.0, the adsorption removal rate and adsorption capacity of  $\text{Pb}^{2+}$  increased from 35.31% and 1.32 mg/g to 99.46% and 3.73mg/g, and the removal rate and capacity of MB increased from 4.22% and 0.16 mg/g to 83.10% and 3.12 mg/g, respectively. This could be related to the surface adsorbent charge. When pH was low, the high concentration of  $\text{H}^+$  in the solution readily protonated the adsorbent surface, causing electrostatic repulsion with  $\text{Pb}^{2+}$ . With a higher pH, the positive charge on the surface of LBM gradually decreased ( $\text{pH}_{\text{pzc}} = 4.1$ , i.e. the surface potential was negative when pH was higher than 4.1). Consequently, the adsorption of  $\text{Pb}^{2+}$  and MB was driven by electrostatic attraction. Further,  $\text{Pb}^{2+}$  continued slowly increasing and levelled off at pH 4.0-5.0, which implies that the extent of protonation on the adsorbent's surface, along with the competitive adsorption between  $\text{H}^+$  and  $\text{Pb}^{2+}$ , was diminished (Ghafil et al., 2024).

The difference can be seen in Fig. S3(b), in which the adsorptive removal of  $\text{Pb}^{2+}$  and CR show different trends. As the pH rose from 1.0 to 5.0, the adsorption removal rate and adsorption capacity of  $\text{Pb}^{2+}$  increased from 45.23% and 1.70 mg/g to 93.15% and 3.49 mg/g, respectively. In contrast, those of CR decreased from 89.163% and 3.34 mg/g to 76.3% and 3.34 mg/g, respectively. This is because MB and CR are different types of ionic dyes, and with the rise in pH, the increase of  $\text{OH}^-$  resulted in electrostatic repulsion between LBM and anionic CR, which were both negatively charged. In addition, one can see by comparing Fig. S3(a) and (b) that pH had a more obvious influence on  $\text{Pb}^{2+}$ -MB. These results prove that electrostatic attraction is important during adsorption. In particular, the change trend of  $\text{Pb}^{2+}$  in the  $\text{Pb}^{2+}$ -CR system is not clear, demonstrating that other non-electrostatic interaction factors also contribute to adsorption, for example,  $\pi$ - $\pi$  packing and hydrogen bonding forces (Li et al., 2024a). In conclusion, an

appropriate increase in pH was favorable for adsorption in the  $\text{Pb}^{2+}$ -MB composite system, while the best pH was 5 for the  $\text{Pb}^{2+}$ -CR composite system.

### 3.4.3 Ionic strength

Ionic strength is another key factor that affects interactions between the adsorbate and interface of an adsorbent. In general, the effect of ionic strength is mainly manifested as (1) changes in the structure of the adsorbent bipolar layer; (2) a decrease in the radius of hydrated ions; and (3) competition for active sites between coexisting ions (Chen et al., 2024a; Wang et al., 2013).

For the  $\text{Pb}^{2+}$ -MB system, the adsorption removal and adsorption capacity of  $\text{Pb}^{2+}$  and MB decreased with the increase of ionic strength (Appendix A Fig. S4(a)). When NaCl increased from 0.01 mol/L to 0.05 mol/L, the adsorption removal and adsorption capacity of  $\text{Pb}^{2+}$  and MB decreased by 1.33%, 0.05 mg/g, and 26.78%, 1.00 mg/g, respectively. This further proves that the surface of LBM is mainly characterized by negative charge. The main reason for these results is that the competition of electrolyte ions caused electrostatic bonding between higher concentrations of  $\text{Na}^+$  and LBM (Abbas et al., 2022; Liu et al., 2022b).

For the  $\text{Pb}^{2+}$ -CR system (Appendix A Fig. S4(b)), the adsorption removal rate and adsorption capacity of  $\text{Pb}^{2+}$  increased slightly with the ionic strength, from 94.83% and 3.56 mg/g to 97.56% and 3.66 mg/g, respectively, after which there was a decrease of 1.27% and 0.05 mg/g; whereas for CR, the adsorption removal rate and adsorption capacity also increased and then decreased slightly with the increase of ionic strength, from 76.87% and 2.88 mg/g to 78.11% and 2.55 mg/g, respectively, and then decreased by 0.91% and 0.03 mg/g. The removal of  $\text{Pb}^{2+}$  and CR decreased slightly with the further increase of ionic strength. This might be due to excess ions forming a barrier between LBM and  $\text{Pb}^{2+}$  and CR (Chanzu et al., 2019; Tang et al., 2020).

Overall, higher ionic strength had less effect on  $\text{Pb}^{2+}$  and CR. In the case of the anionic dye CR, the presence of  $\text{Na}^+$  neutralized the anionic negative charge of CR and weakened the electrostatic repulsion; thus it facilitated the migration of the anionic

dye from the solution to the surface of LBM. In addition, the “salt-out” effect promoted adsorption of CR (Liu et al., 2022a). The increase in CR adsorption promoted adsorption of  $\text{Pb}^{2+}$  to a certain extent. This is due to the bridge bonding between  $\text{Pb}^{2+}$  and CR. This synergistic effect was also clarified subsequently. In both composite systems, the adsorption removal of  $\text{Pb}^{2+}$  exhibited good performance, which also verified the existence of chemisorption between  $\text{Pb}^{2+}$  and LBM. We speculate that the adsorption force of  $\text{Pb}^{2+}$  and LBM was too strong to allow desorption. In conclusion, appropriate reduction of ionic strength for the  $\text{Pb}^{2+}$ -MB composite system, but an increase of ionic strength for the  $\text{Pb}^{2+}$ -CR composite system, are conducive to co-adsorption.

### 3.4.4 System temperature

The effect of temperature can be observed in Appendix A Fig. S5. In the  $\text{Pb}^{2+}$ -MB system, LBM had a high adsorption removal rate for  $\text{Pb}^{2+}$  between 10-50 °C. This implies that LBM has a strong affinity for  $\text{Pb}^{2+}$ , with a large number of unoccupied adsorption sites at the beginning which can adsorb rapidly in spite of the lower temperature. As the temperature rose, the adsorption removal rate of  $\text{Pb}^{2+}$  showed a slightly increasing trend, and the adsorption removal and adsorption capacity increased from 99.11% and 3.72 mg/g to 99.58% and 3.73 mg/g, respectively; the adsorption efficiency reached the maximum at 40 °C, with the adsorption removal and adsorption capacity increasing from 49.16% and 1.84 mg/g to 84.336% and 3.16 mg/g, respectively. They decreased slightly at 50 °C (by 10.87% and 0.41 mg/g). For the  $\text{Pb}^{2+}$ -CR system, the adsorption removal and adsorption capacity of  $\text{Pb}^{2+}$  and CR increased with increasing temperature from 70.51% and 2.64 mg/g to 94.96% and 3.56 mg/g and from 48.50% and 1.87 mg/g to 78.37% and 2.94 mg/g, respectively.

The high reaction temperature enhanced thermal movement of molecules and promoted their adsorption capacity. In addition, the increase in temperature led to a decrease in the viscosity of the adsorption solution, thus facilitating the adsorption removal rate. Another explanation for the slight decrease of adsorption removal and adsorption capacity for MB at 50 °C may be the increase in molecular mobility that

promoted desorption of previously adsorbed MB (Abegunde et al., 2024). Alternatively, at higher temperatures, the hydrogen bonds between MB and LBM might be severed, leading to reduced adsorption capacity, as found by Aryee (Aryee et al., 2022). The increase in the system temperature generally promoted the adsorption capability of LBM, which further highlighted the fact that within a certain temperature range, adsorption of  $\text{Pb}^{2+}$ , MB, and CR is mainly a heat-absorbing process, in concordance with the laws of adsorption thermodynamics. In brief, an appropriate increase in temperature for  $\text{Pb}^{2+}$ -MB/CR composite systems is favorable for adsorption.

### 3.5 Interactions between coexisting pollutants in composite systems

#### 3.5.1 Interaction between $\text{Pb}^{2+}$ and MB in the composite system

The results of the interaction between  $\text{Pb}^{2+}$  and MB in simultaneous adsorption are shown in Appendix A Fig. S6. Fig. S6(a) illustrates that with an increase in MB concentration (50 mg/L, 100 mg/L, 150 mg/L), the adsorption capacity of  $\text{Pb}^{2+}$  at different concentrations (50 mg/L, 100 mg/L, 150 mg/L) decreased by 0.93 mg/g, 1.82 mg/g, and 2.04 mg/g, respectively. Meanwhile, with an increase in the concentration of  $\text{Pb}^{2+}$  (50 mg/L, 100 mg/L, 150 mg/L), the adsorption capacity of MB at different concentrations (50 mg/L, 100 mg/L, 150 mg/L) decreased by 2.53 mg/g, 3.70 mg/g, and 6.43 mg/g, respectively (Fig. S6(c)). We can conclude that in the composite system,  $\text{Pb}^{2+}$  and MB had the same negatively charged adsorption sites; thus there were different degrees of antagonism between them. Because some active sites of LBM might be occupied after the adsorption of one component, the spatial site resistance is enhanced, which leads to the adsorption of the other component being further reduced. Certainly, the inhibition of adsorption of another component became more obvious as the concentration of the competing component increased. The reason could be that increasing the concentration of the composite system provided a higher possibility of contact between the active site and the adsorbate. When the adsorption sites on the LBM surface were almost occupied, this

caused large numbers of adsorbate ions to compete for the relatively small number of available sites until adsorption saturation was reached.

Cationic dyes and heavy metal ions mainly involve cationic complexation with each other in simultaneous removal, so that their diffusion rate to LBM was low and they competed with each other (Visa et al., 2010). Therefore, there was hardly any synergistic or independent adsorption such as we found in the composite system of  $\text{Pb}^{2+}$  and MB. On the one hand, in view of the electronegativity of LBM, the same positive charge of  $\text{Pb}^{2+}$  and MB made it possible to have similar adsorption sites. On the other hand,  $\text{Pb}^{2+}$  would also have electrostatic repulsion with MB. Meanwhile, the inhibitory effect of the two components was different, and the adsorption removal rate of  $\text{Pb}^{2+}$  was always high, above 96.94%; in other words, the inhibitory effect of MB on the adsorption removal rate of  $\text{Pb}^{2+}$  was not obvious. This indicates that LBM had enough adsorption sites for  $\text{Pb}^{2+}$  to adsorb at this concentration. Compared with MB, the adsorption removal rate of  $\text{Pb}^{2+}$  by LBM was greater. The above implies that adsorption removal of  $\text{Pb}^{2+}$  by LBM was in a favorable position in the competitive adsorption. This outcome stems from the variations in the electronic structure and size of  $\text{Pb}^{2+}$  and MB. Research has indicated that ions with higher charge densities tend to have higher exchange rates. The positive charge of  $\text{Pb}^{2+}$  was greater than the number of MB ions, while the spatial structure of  $\text{Pb}^{2+}$  was smaller than that of MB. These characteristics were more favorable for ion exchange (Wang and Ariyanto, 2007). A comparable observation was made by Liang *et al* regarding the competitive adsorption between MB and  $\text{Cu}^{2+}$ , which they investigated by utilizing magnetic graphene oxide/alginate microbeads (mGO/CA). They found that since the hydrated ionic radius of  $\text{Cu}^{2+}$  was smaller than that of MB and the charge density was higher than that of  $\text{Cu}^{2+}$ , mGO/CA could adsorb much more  $\text{Cu}^{2+}$  than MB (Liang *et al*, 2020). Alinezhad *et al* obtained a maximum adsorption capacity of  $\text{Hg}^{2+}$  higher than that of MB in binary aqueous solution by using new polymer composites (Alinezhad et al., 2020).

At a lower  $\text{Pb}^{2+}$  concentration (50 mg/L), the  $R_{q, \text{pb}}$  was close to 1.0, so the MB had less effect on the

adsorption of  $\text{Pb}^{2+}$  (Fig. S6(b)). This meant that the adsorption sites of LBM were relatively adequate under these conditions, even though in the presence of competing components, LBM still removed  $\text{Pb}^{2+}$ . However, as the concentration of  $\text{Pb}^{2+}$  increased,  $0.72 < R_{q, \text{Pb}} < 0.97$ , which further shows that the inhibitory effect was strengthened when  $\text{Pb}^{2+}$  concentration was higher. Combined with  $0.39 < R_{q, \text{MB}} < 0.64$ , the inhibitory effect of MB adsorption by  $\text{Pb}^{2+}$  was stronger. In a word, LBM had a stronger affinity for  $\text{Pb}^{2+}$  than MB in the composite system.

### 3.5.2 Interaction between $\text{Pb}^{2+}$ and CR in the composite system

The results of the interaction between  $\text{Pb}^{2+}$  and CR in simultaneous adsorption are shown in Appendix A Fig. S7. In Fig. S7(a), one can see that with the increase of CR concentration (50 mg/L, 100 mg/L, 150 mg/L), the adsorption capacity of  $\text{Pb}^{2+}$  at different concentrations (50 mg/L, 100 mg/L, 150 mg/L) increased by 0.15 mg/g, 0.96 mg/g, and 2.07 mg/g, respectively. With the increase in  $\text{Pb}^{2+}$  concentration (50 mg/L, 100 mg/L, 150 mg/L), the adsorption capacity of MB at different concentrations (50 mg/L, 100 mg/L, 150 mg/L) increased by 1.11 mg/g, 2.38 mg/g, and 5.94 mg/g, respectively (Fig. S7(c)). Thus there was a synergistic effect between CR and  $\text{Pb}^{2+}$ . Clearly, when the concentration of one component increased, it promoted the adsorption process of the other component within a certain concentration range, gradually enhancing the promotion effect. The subsequent process predominantly contributed to the simultaneous adsorption of anionic dyes and heavy metal ions. Initially, the anionic dyes had the potential to engage in complexation with the heavy metal ions and be adsorbed. Then, a certain component preferentially occupied the active site and acted as a bridge to promote the adsorption of other components through coordination, complexation, or electrostatic attraction; for example, the carboxyl, amino, or sulfonic acid groups of the dye molecule could be used as binding sites (Qin et al., 2019). Therefore, in the  $\text{Pb}^{2+}$ -CR composite system, LBM could still effectively adsorb  $\text{Pb}^{2+}$  and CR, and the adsorption effect on  $\text{Pb}^{2+}$  was better. From the viewpoint of charge conservation, after the adsorption of positively

charged  $\text{Pb}^{2+}$ , the concentration of  $\text{H}^+$  in the solution increased, and so did the pH, which resulted in gradual expression of a positively charged state on the surface of LBM. Then electrostatic attraction facilitated adsorption of CR. This synergistic adsorption effect might lead to preferential adsorption of  $\text{Pb}^{2+}$ , and  $\text{Pb}^{2+}$  played the role of the “LBM- $\text{Pb}^{2+}$ -CR” bridge, which enhanced the adsorption efficiency of CR (Liu et al., 2023a). In addition, some of the  $\text{Pb}^{2+}$  could bind to CR, and LBM with a negatively charged surface had enough adsorption sites for  $\text{Pb}^{2+}$  at lower initial concentrations. The parts of CR and LBM with negative charge repelled each other and CR was retained in solution, so sulfonic acid groups on CR in solution could interact with  $\text{Pb}^{2+}$ . At the lower initial concentration of 50 mg/L,  $R_{q, \text{Pb}} < 1.0$ , possibly because LBM had an adequate number of adsorption sites for  $\text{Pb}^{2+}$  and the synergistic effect of the coexisting CR was not significant. With the increase of initial  $\text{Pb}^{2+}$  concentration,  $1.08 < R_{q, \text{Pb}} < 1.38$ , and the promotion effect of CR showed an upward trend. This synergistic relationship was also corroborated by the fact that  $1.05 < R_{q, \text{CR}} < 1.35$ , as shown in Fig. S7(d).

### 3.6 Influence of coexisting cations and anions on adsorption in the composite systems

Printing and dyeing wastewater usually contains other complex components which come from various chemical auxiliaries used in dye production and the dyeing process. Therefore, it contains relatively high concentrations of salt substances such as  $\text{Na}^+$ ,  $\text{Mg}^{2+}$ ,  $\text{K}^+$ ,  $\text{NO}_3^-$ ,  $\text{SO}_4^{2-}$ , and  $\text{PO}_4^{3-}$ . These cations and anions usually affect adsorption. Therefore, it is of great significance to explore the interference effect of common co-existing ions on adsorption. Appendix A Fig. S8-9 shows the influence of interfering ions with an ionic strength of 0.03 mol/L in  $\text{Pb}^{2+}$ -MB/CR composite systems.

In the  $\text{Pb}^{2+}$ -MB composite system, when cations and anions were added, adsorption and removal of  $\text{Pb}^{2+}$  were more strongly inhibited by cations than anions; the addition of anions had almost no effect on  $\text{Pb}^{2+}$ . The coexisting cations had an obvious effect on the adsorption of MB compared to that of  $\text{Pb}^{2+}$ . For MB, the adsorption removal rate decreased when cations were added. When the ionic strength of  $\text{Na}^+$ ,

$\text{Mg}^{2+}$ , or  $\text{K}^+$  was 0.03 mol/L, the adsorption removal rate of MB decreased by 7.88%, 41.38%, and 48.81%, respectively. However, when anions were added, the adsorption removal rate of MB increased by 0.54%, 1.02%, and 2.81%, respectively. The explanation is that cations and MB have the same positive charge, so they have similar adsorption sites. Cations can occupy the active site of LBM and change its surface electrical properties (Li et al., 2023). However, the addition of anions produced more negative ions sites on the LBM surface, which strengthened the electrostatic attraction with cationic MB. Therefore, the cations inhibited adsorption removal of MB. At the same time, the impact of interfering cations on MB was  $\text{Na}^+ < \text{Mg}^{2+} < \text{Ca}^{2+}$ , because the electronegativity as well as the charge of the coexisting ions influenced the adsorption affinity between LBM and MB. Since the charge quantity of  $\text{Na}^+ < \text{Ca}^{2+}$  and  $\text{Mg}^{2+}$ , and the electronegativity of  $\text{Na}^+$  (0.93)  $< \text{Ca}^{2+}$  (1.00) and  $\text{Mg}^{2+}$  (1.31),  $\text{Ca}^{2+}$  and  $\text{Mg}^{2+}$  had stronger hydration capacities and electrostatic attraction to occupy the active sites easily (Jiang et al., 2022; Liu et al., 2023b). Thus,  $\text{Ca}^{2+}$  and  $\text{Mg}^{2+}$  competed more strongly with MB. The influence of interfering anions on MB was in the order of  $\text{NO}_3^- < \text{SO}_4^{2-} < \text{PO}_4^{3-}$ , indicating that ions with higher valence states had greater potential than univalent ions and carried more negative charge, resulting in a greater influence on MB adsorption (Brahma and Saikia, 2022).

In the  $\text{Pb}^{2+}$ -CR composite system, the addition of cations and anions promoted adsorption of  $\text{Pb}^{2+}$ , with slight increases of 0.78%, 2.77%, 1.92%, 0.68%, 1.17%, and 3.75% after adding 0.03 mol/L of  $\text{Na}^+$ ,  $\text{Mg}^{2+}$ ,  $\text{Ca}^{2+}$ ,  $\text{NO}_3^-$ ,  $\text{SO}_4^{2-}$ , and  $\text{PO}_4^{3-}$ . The addition of cations was beneficial to the adsorption of  $\text{Pb}^{2+}$ , as the increased adsorption of CR enhanced the negative charge on the surface of LBM, providing additional adsorption sites. The influence of coexisting anions on  $\text{Pb}^{2+}$  was  $\text{NO}_3^- < \text{SO}_4^{2-} < \text{PO}_4^{3-}$ .  $\text{SO}_4^{2-}$  and  $\text{PO}_4^{3-}$  easily formed stable precipitation with  $\text{Pb}^{2+}$ , which reduced the concentration of  $\text{Pb}^{2+}$  in the form of precipitation; thus LBM exhibited a higher adsorption removal rate of  $\text{Pb}^{2+}$ . For CR, when the ionic strength of  $\text{Na}^+$ ,  $\text{Mg}^{2+}$ , and  $\text{K}^+$  was 0.03 mol/L, the adsorption removal rate of CR increased by 7.90%, 12.46%, and 19.78%, respectively. This is due to the fact that the

cations in the solution neutralized the repulsive force between the negatively charged LBM and CR. This finding is in alignment with the aforementioned research outcomes regarding the impact of ionic strength. In addition,  $\text{Mg}^{2+}$  and  $\text{Ca}^{2+}$  had higher positive charge than  $\text{Na}^+$ , which explains why  $\text{Mg}^{2+}$  and  $\text{Ca}^{2+}$  had a stronger promotion effect, and the “salt-out effect” generated by  $\text{Mg}^{2+}$  and  $\text{Ca}^{2+}$  made the precipitated CR more easily adsorbed (Wu et al., 2021). He et al. also found that  $\text{Ca}^{2+}$ ,  $\text{Na}^+$ , and  $\text{K}^+$  gave activated carbon a positive charge, thus enhancing electrostatic interactions between the adsorbent and CR with high adsorption of CR (He et al., 2023). In contrast, we found that the anions hindered the adsorption of CR. The influence was in the order of  $\text{NO}_3^- < \text{SO}_4^{2-} < \text{PO}_4^{3-}$ , and there was a decrease of 15.10%, 19.25%, and 22.91% after adding the 0.03 mol/L  $\text{NO}_3^-$ ,  $\text{SO}_4^{2-}$ , and  $\text{PO}_4^{3-}$ . Because  $\text{NO}_3^-$ ,  $\text{SO}_4^{2-}$ ,  $\text{PO}_4^{3-}$ , and CR are anions, they could compete for similar adsorption sites, while  $\text{NO}_3^-$ , which had a lower charge density, was less competitive (Sumanta et al., 2021). Furthermore,  $\text{SO}_4^{2-}$  competed with sulfonic acid groups of CR molecules.  $\text{PO}_4^{3-}$  formed  $\text{H}_2\text{PO}_4^-$ ,  $\text{HPO}_4^{2-}$ , and  $\text{PO}_4^{3-}$  through ionization, which consumed more adsorption sites than other compounds (Brahma and Saikia, 2022; Wu et al., 2022). This resulted in greater inhibition of CR adsorption.

The above results indicate that LBM has the potential to simultaneously adsorb  $\text{Pb}^{2+}$ , MB, and CR in actual wastewater treatment, especially since it maintains a good adsorption removal rate for  $\text{Pb}^{2+}$ . They also confirm that electrostatic action plays a crucial role in this adsorption process.

### 3.7 Desorption characteristics and recycling potential of LBM after adsorption

Optimal recyclability and stability are important features of ideal adsorbent materials (Wang et al., 2024a). In order to achieve stability and the potential for LBM regeneration and recycling after adsorption, we tried three different desorbents. The outcome is shown in Appendix A Fig. S10.

Currently, the usual desorption methods for the regeneration cycle of biomass materials include acid desorption and alkali desorption (Himanshu, 2021).  $\text{H}^+$  displaces large amounts of heavy metal ions and

dyes due to competitive adsorption, so regeneration is generally achieved by treating adsorbents in an inorganic acid solution (Lan et al., 2023).

In the  $\text{Pb}^{2+}$ -MB composite system, the desorption rate of  $\text{Pb}^{2+}$  was 12.32%, 12.96%, and 9.68%, and the desorption rate of MB was 68.4%, 76.53%, and 83.81% when  $\text{H}_2\text{SO}_4$ ,  $\text{HNO}_3$ , and  $\text{HCl}$  were respectively used as desorbents. In the  $\text{Pb}^{2+}$ -CR composite system, the desorption rate of CR was 0%, while the desorption rate of  $\text{Pb}^{2+}$  was also low. The desorption rate of 0.1 mol/L  $\text{H}_2\text{SO}_4$ , 0.1 mol/L  $\text{HNO}_3$ , and 0.1 mol/L  $\text{HCl}$  as desorbents was 5.94%, 7.16%, and 5.45%, respectively. The desorption rates of different systems were determined by the structural features of the LBM and the properties of the adsorbate. Biomass with rich functional groups plays a key role in the strong complex adsorption of cationic  $\text{Pb}^{2+}$  (Li et al., 2024b). Therefore, complexation generated more lead complexes, while a MB complexation reaction was not evident, resulting in a higher desorption rate for MB than  $\text{Pb}^{2+}$ . In addition to the possible complexation and chelation between LBM and  $\text{Pb}^{2+}$ , LBM also contained more minerals such as  $\text{Ca}_3(\text{PO}_4)_2$  and  $\text{Fe}_2\text{Ti}_3\text{O}_9$ , which formed insoluble precipitates with  $\text{Pb}^{2+}$  by exchanging ions and removing them as microprecipitation. This led to a portion of the LBM being difficult to desorb, such that the desorption of  $\text{Pb}^{2+}$  was much less than that of MB. Compared with the  $\text{Pb}^{2+}$ -MB composite system, desorption of  $\text{Pb}^{2+}$  in the presence of CR was less, due to the establishment of robust complexes between  $\text{Pb}^{2+}$  and CR with sulfonic acid groups through electrostatic interaction and coordination (Tran et al., 2022). Meanwhile, the other part of the LBM that adsorbed  $\text{Pb}^{2+}$  suffered from the promotion of CR, which firmly bonded the  $\text{Pb}^{2+}$  to the LBM. This explains why  $\text{Pb}^{2+}$  and CR were more difficult to desorb, and why the LBM that adsorbed  $\text{Pb}^{2+}$  and CR had better stability. In view of this, LBM could be utilized as a disposable material for simultaneous adsorption removal of  $\text{Pb}^{2+}$ -CR. Although the  $\text{Pb}^{2+}$ -MB composite system could be desorbed, the desorption rate was not high and there was a substantial difference between the two systems. The time and cost required for the desorption process lead to the conclusion that treatment LBM as a treatment in the  $\text{Pb}^{2+}$ -MB composite system

is also more suitable as a disposable material. In addition, attention should be paid to avoiding release of  $\text{Pb}^{2+}$ , MB, and CR in the treatment of post-adsorption LBM material, because the material had a certain desorption rate, it meant that pollutants might be released from the adsorbent surface into the environment when rainwater leached, leading to secondary pollution.

The mechanism of the adsorption process is also closely related to the desorption process. If an adsorbent can be desorbed with water alone, then the adsorption bond is usually weak, while desorption with an acid or alkali desorbent is more difficult, showing that stronger chemisorption has occurred. LBM clearly exhibited chemisorption of  $\text{Pb}^{2+}$ , MB, and CR.

### 3.8 Characterization of adsorption behavior

#### 3.8.1 Surface characteristics of LBM before and after adsorption in composite systems

SEM was used to scan the surface characteristics shown in Fig. 3. It is clear that the surface of LBM without adsorption presents an irregular and uneven cluster-like morphology at the microscopic level, rich in crystalline substances. The various particles also have pores of different sizes (Fig. 3(a)). The uneven folds and porous structure could provide abundant active adsorption sites and promote the efficiency of interactions in pores.

After adsorption in  $\text{Pb}^{2+}$ -MB/CR composite systems (Fig. 3), LBM has an obvious honeycomb structure and rough cavities, and many sheets and broken structures have formed on the surface because  $\text{Pb}^{2+}$ , MB, and CR have entered the adsorption sites and destroyed the surface structure. Due to the interaction between the adsorbates and LBM, the adsorbates aggregated on the surface of LBM, which made the surface rougher and looser and formed irregular dispersed shapes. The specific surface area and pore volume of LBM are small; hence the pore structure was not the primary controlling factor for adsorption with LBM. The primary factor was surface adsorption, and these results coincide with those obtained via SEM.

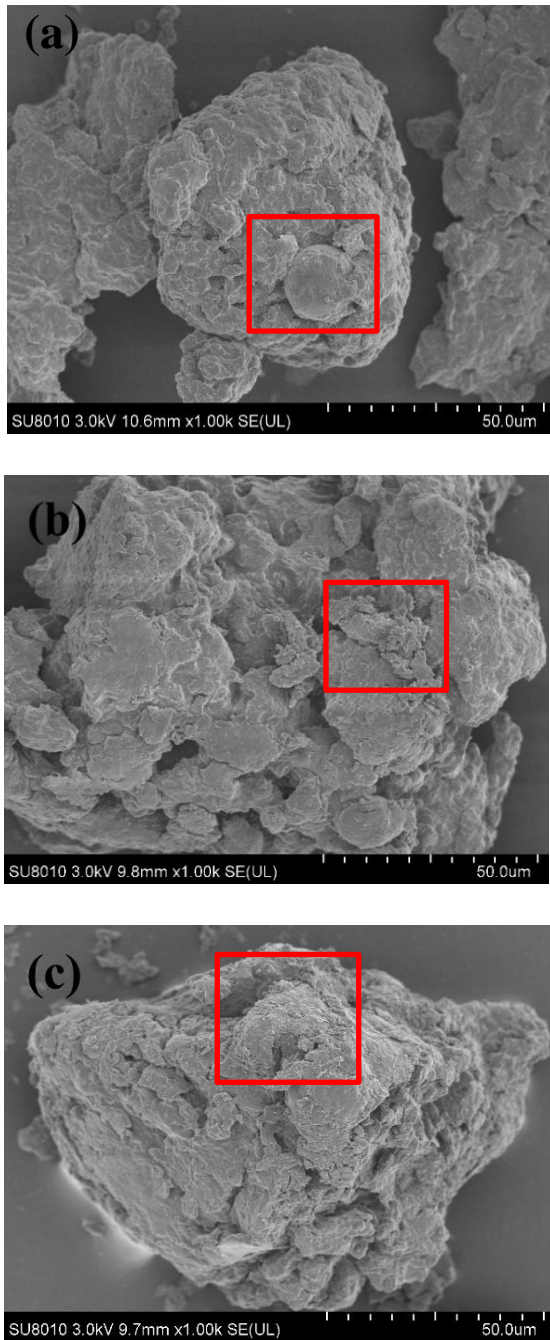


**Fig.3** Surface characteristics of LBM(a), after adsorption of  $Pb^{2+}$ -MB (b) and  $Pb^{2+}$ -CR (c) composite systems

### 3.8.2 XRD characteristics of LBM before and after adsorption in the composite systems

In order to understand the contributions of mineral components in LBM during the adsorption process, we used XRD to analyze LBM before and after adsorption in the composite systems, and the results are shown in Fig. 4. LBM before and after adsorption

has obvious characteristic peaks at  $27.40^\circ$ ;  $28.28^\circ$ ;  $36.10^\circ$ ;  $41.10^\circ$ ;  $43.94^\circ$ ;  $54.20^\circ$ ;  $56.40^\circ$ ;  $62.61^\circ$ ;  $63.88^\circ$ ;  $68.80^\circ$ ; and  $69.61^\circ$ , which corresponds to the characteristic peaks of  $TiO_2$ . In addition,  $27.40^\circ$  indicates the characteristic diffraction peak of  $SiO_2$ .  $36.81^\circ$ ;  $39.11^\circ$ ;  $41.23^\circ$ ;  $54.30^\circ$ ; and  $56.61^\circ$  indicate the characteristic diffraction peaks of  $Fe_2Ti_3O_9$ .  $39.11^\circ$  is the characteristic diffraction peak of  $Ca_3(PO_4)_2$ , and  $35.96^\circ$  and  $56.61^\circ$  are the characteristic diffraction peaks of  $CaCO_3$ .

Compared with the post-adsorption LBM, the corresponding characteristic peaks shown by LBM before adsorption were sharper and the peak height was higher, meaning that the crystallinity of related minerals was higher. After adsorption, the peak heights of the relative features of LBM decreased, and so did the intensity of the peaks, due to the adsorption reaction between the mineral surfaces in the LBM and the adsorbate molecules during the adsorption process changing the surface structure of the LBM. This caused the mineral crystals of the aforementioned minerals to change to an amorphous and loose structure, which resulted in a decrease in the crystallinity of the minerals in the outer layer of the LBM. The small peak at about  $28.28^\circ$  represents  $TiO_2$ , which decreased significantly after adsorption, indicating that it played an important role in adsorption. Moreover,  $SiO_2$  and  $TiO_2$  had many surface adsorption sites.  $Pb^{2+}$ , MB, and CR were adsorbed in the vacancy through physical adsorption, and hydroxyl was produced by hydration to act on  $Pb^{2+}$  and both dyes. In addition,  $SiO_2$ ,  $Fe_2Ti_3O_9$ ,  $TiO_2$ , and  $Ca_3(PO_4)_2$  facilitated the adsorption of  $Pb^{2+}$ , MB, and CR by LBM through bridge bonds. The  $Ca^{2+}$  in LBM reacted with the sulfonic acid groups in the anionic dye CR, resulting in precipitation of adsorption. In LBM, the anionic phosphate in  $Ca_3(PO_4)_2$  also reacted with MB and  $Pb^{2+}$ , forming a stable structure. This also explains the incomplete or very low desorption of MB, CR, and  $Pb^{2+}$  after adsorption.



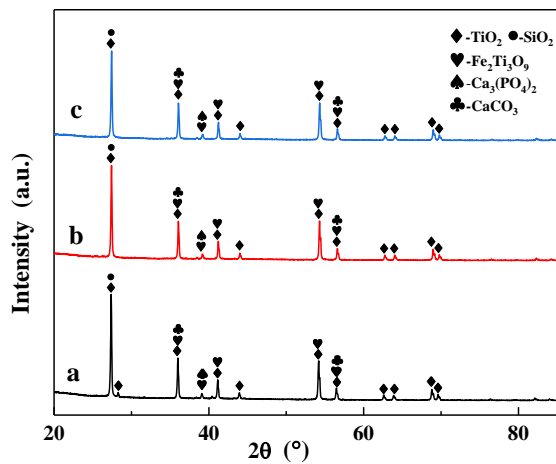


**Fig.4** XRD characteristics of LBM in the  $\text{Pb}^{2+}$ -MB/CR composite system before and after adsorption (a, before adsorption, b, after adsorption of  $\text{Pb}^{2+}$ -MB, c, after adsorption of  $\text{Pb}^{2+}$ -CR)

### 3.8.3 FTIR characteristics of LBM before and after adsorption in the composite systems

LBM contains abundant C, N, O, H and other elements and organic matter, indicating that it contains more organic matter such as microbial residues and microbial metabolites, which would inevitably participate in the adsorption process. In order to understand the adsorption action between the relevant functional groups on LBM and the adsorbent, we used FTIR to analyze the LBM before and after adsorption (see Fig. 5).

In the composite systems, due to the interactions between different functional groups and components, the different types of adsorption processes were complicated. It can be seen from Fig. 5 that the infrared absorption peaks of most groups shifted, which implies that they reacted with the adsorbate. For the  $\text{Pb}^{2+}$ -MB composite system, at a peak of  $3318\text{ cm}^{-1}$ , the stretching vibration peaks of -OH, N-H shifted to  $3394\text{ cm}^{-1}$ . The C=O stretching vibration peak shifted to  $1724\text{ cm}^{-1}$ , the -COOH and C=N stretching vibration peaks shifted to  $1685\text{ cm}^{-1}$ , and the C=C skeletal vibration peak shifted to  $1546\text{ cm}^{-1}$ . Meanwhile, for the  $\text{Pb}^{2+}$ -CR composite system, the O-H, N-H stretching vibration peaks at  $3318\text{ cm}^{-1}$  shifted to  $3415\text{ cm}^{-1}$ . The peak at  $1685\text{ cm}^{-1}$  can be ascribed to -COOH stretching vibration groups. The C=N stretching vibration groups shifted to  $1687\text{ cm}^{-1}$  and

the C=C skeleton vibration peak of  $1546\text{ cm}^{-1}$  shifted to  $1550\text{ cm}^{-1}$ . This proves that the abundant amino and carboxyl groups of LBM can form strong complexations with  $\text{Pb}^{2+}$  and thus have a high adsorption capacity for  $\text{Pb}^{2+}$ . In addition, O-H (as an electron donor) can complex with  $\text{Pb}^{2+}$ , MB, and CR (Kyzas et al., 2015; Li et al., 2019a). Thus the hindering effect of complexes was also one of the reasons for the decrease in the adsorption removal rate in the composite system. Combining the molecular structure figures of both dyes (Appendix A Fig. S1) demonstrated the presence of numerous N-containing groups in MB which acted as hydrogen-bond acceptors. This was linked to the creation of hydrogen bonds with the oxygen-bearing functional groups on LBM, such as hydroxyl, carboxyl, and carbonyl groups. The  $-\text{NH}_2$ -,  $-\text{SO}_3^-$ , and  $-\text{N}=\text{N}-$  groups carried by CR could also formed hydrogen bonds with the above-mentioned functional groups on LBM (Li et al., 2019c; Zhang et al., 2023a). The bending vibration peak of  $-\text{CONH}_2$  at  $1378\text{ cm}^{-1}$  and  $1230\text{ cm}^{-1}$  after adsorption of the  $\text{Pb}^{2+}$ -MB composite system shifted to higher wave numbers, and the C-H stretching vibration peak at  $506\text{ cm}^{-1}$  weakened significantly and shifted to  $515\text{ cm}^{-1}$ . This represented the C-H bending vibration peak at  $1459\text{ cm}^{-1}$ , which shifted to  $1463\text{ cm}^{-1}$  after adsorption of the  $\text{Pb}^{2+}$ -CR composite system, and the C-H stretching vibration peak at  $506\text{ cm}^{-1}$  disappeared, which we attribute to complexing reactions during adsorption. Moreover,  $\text{Pb}^{2+}$ , MB, and CR were adsorbed by hydroxyl groups because of electrostatic interactions, and dyes with aromatic rings and the C=C double bond carried by CR formed a  $\pi$ - $\pi$  bonding system with the LBM. Some characteristic peaks such as  $-\text{CH}_2$  stretching vibration and C=C skeleton vibration peaks were not significantly shifted, however, it is clear that the strength of infrared characteristic peaks was enhanced after adsorption in the two composite systems. Meanwhile, the strength of infrared characteristic peaks of -OH and N-H groups, which were significantly shifted, was also enhanced. These results indicate that some organic substances, i.e., MB and CR, were adsorbed on the LBM surface. This is because in the composite system, the possible interactions between adsorbates and LBM resulted in an increase in the above groups from adsorbed MB or



CR on the LBM surface.

In summary, the positively charged groups (e.g., -OH) and negatively charged groups (e.g., -COOH) carried by LBM achieved synergistic removal of  $\text{Pb}^{2+}$  and anionic dyes in water by electrostatic attraction. Vibrational changes in the O-H, N-H, and -COOH stretching vibration peaks indicate complexation with  $\text{Pb}^{2+}$ , MB, and CR; N groups also played an important role as hydrogen receptors and hydrogen bonds with oxygen-containing functional groups such as O-H, -COOH, and C=O carried by LBM. In addition, O-H, C-H stretching vibration peaks, the C=N stretching vibration peak, and the C=C skeleton vibration peak could be combined with the MB and CR through non-covalent interactions such as CH- $\pi$  or  $\pi$ - $\pi$  conjugated effects. This proves that functional groups such as hydroxyls, aminos, carbonyls, alkyls, and carboxyls, interact with an adsorbent and make important contributions to competitive adsorption.

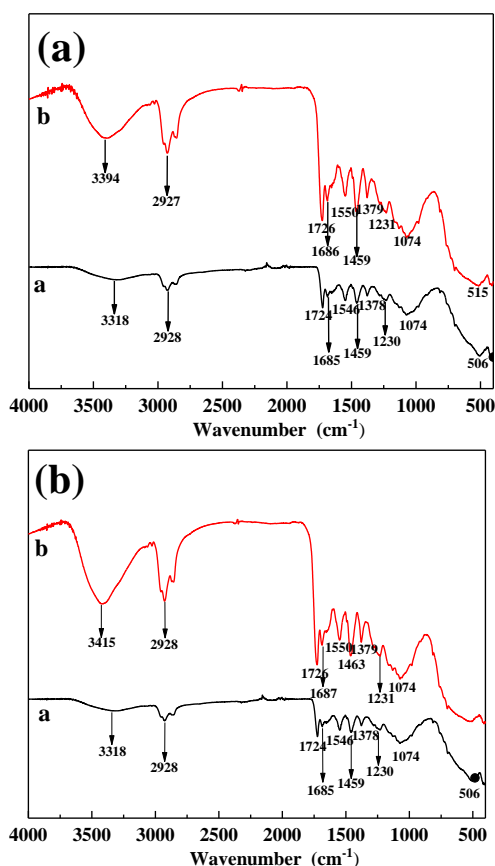


**Fig.5** FTIR characteristics before and after LBM adsorption in  $\text{Pb}^{2+}$ -MB (a) and  $\text{Pb}^{2+}$ -CR (b) composite systems (a, before adsorption, b, after adsorption)

## 4 Conclusions

LBM is a suitable, novel material for simultaneous adsorption removal of heavy metals and dyes in the composite system of printing and dyeing wastewater. The adsorption kinetics of  $\text{Pb}^{2+}$ -MB/CR composite systems can be effectively characterized by the pseudo-second-order kinetic model ( $R^2 > 0.99$ ), which is dominated by the chemisorption process. In the  $\text{Pb}^{2+}$ -MB composite system, both the Langmuir isothermal adsorption model ( $R^2 > 0.97$ ) and Freundlich isothermal adsorption model ( $R^2 > 0.95$ ) better describe the isothermal adsorption characteristics of  $\text{Pb}^{2+}$  and MB ( $R^2 > 0.97$ ), while only the Freundlich isothermal adsorption model accurately describes the isothermal adsorption characteristics of  $\text{Pb}^{2+}$  and CR in the  $\text{Pb}^{2+}$ -CR composite system ( $R^2 > 0.90$ ). In the  $\text{Pb}^{2+}$ -MB composite system, the adsorption is antagonistic with similar adsorption sites. However, the adsorption is synergistic with different adsorption sites in the  $\text{Pb}^{2+}$ -CR composite system, which leads to a higher simultaneous adsorption capacity with a higher initial  $\text{Pb}^{2+}$ -CR concentration than that of  $\text{Pb}^{2+}$ -MB. In the  $\text{Pb}^{2+}$ -MB/CR composite systems, the LBM dosage and system temperature appropriately increase within a certain range, which contributes to the simultaneous adsorption removal of  $\text{Pb}^{2+}$  and MB or  $\text{Pb}^{2+}$  and CR. The optimal solid-liquid ratio and temperature are 1:75 and 30 °C. The adsorption and removal rates of  $\text{Pb}^{2+}$  and MB were 99.98% and 90.49%, respectively, and those of  $\text{Pb}^{2+}$  and CR were 93.99% and 77.39%, respectively, in (50, 50) mg/L of  $\text{Pb}^{2+}$ -MB/CR composite systems under these conditions. The adsorption removal of  $\text{Pb}^{2+}$  and MB increases with the pH level and decreases as the ionic strength increases, while the removal rate of CR shows an opposite trend, slowly decreasing with the increase of pH and increasing with the increase of ionic strength.

The coexisting cation and anion types have a limited effect on the simultaneous adsorption removal of  $\text{Pb}^{2+}$ , MB, and CR. In the  $\text{Pb}^{2+}$ -MB composite system, the desorption rate of LBM-adsorbed  $\text{Pb}^{2+}$  and MB was lower than 12.96% and higher than 68.4%, respectively, with a large difference in the

desorption rate; whereas in the Pb<sup>2+</sup>-CR composite system, the desorption rate of LBM-adsorbed Pb<sup>2+</sup> and CR was lower than 7.16%. indicating that LBM-adsorbed Pb<sup>2+</sup> and CR had good stability. Therefore, based on the different adsorption characteristics of LBM in the two systems, we suggest that it could be utilized as a disposable material for simultaneous adsorption and removal of Pb<sup>2+</sup>-MB/CR composite systems. In addition, the structure and various inorganic and organic components of LBM contribute to simultaneous adsorption removal. The characterization results reveal that the adsorption of the two composite systems is controlled by complex interactions involving hydrogen bonding, complexations,  $\pi$ - $\pi$  bonding interactions, and electrostatic interactions.

### Acknowledgments

A Project Supported the National Key Research and Development Project of China (2023YFD1702003, 2023YFC3709001)

### Author contributions

Xiaomei Xie and Min Liao conceived the idea. Xiaomei Xie and Min Liao designed the research. Xinyue LU, Hao QIU, Feng YUAN, Zhe LUO, Chunlin FAN performed the experiment. Xiaomei Xie, Xinyue LU and Min Liao analyzed the data and wrote the manuscript. All authors contributed to the discussion of the manuscript.

### Conflict of interest

Xinyue LU, Min LIAO, Xiaomei XIE, Hao QIU, Feng YUAN, Zhe LUO, Chunlin FAN declare that they have no conflict of interest.

### References

- Abbas K, Fazel MM, Kobra S, Sara H, et al., 2022. Equilibrium and Thermodynamic Studies on the Biosorption of Lead (II) by Living and Nonliving Biomass of *Penicillium notatum*. *Journal of Chemistry*, 2022: 3109212. <https://doi.org/10.1155/2022/3109212>
- Abbasi A, Ahmad I, Gawad HHaE, et al., 2024. Appraisal of the adsorption potential of novel modified gellan gum nanocomposite for the confiscation of methylene blue and malachite green. *International Journal of Biological Macromolecules*, 259(P1): 129221. <https://doi.org/10.1016/j.ijbiomac.2024.129221>
- Abegunde SM, Olasehinde EF, Adebayo MA, 2024. Green synthesis of ZnO nanoparticles using *Nauclea latifolia* fruit extract for adsorption of Congo red. *Hybrid Advances*, 5: 100164. <https://doi.org/10.1016/j.hybadv.2024.100164>
- Alinezhad H, Zabihi M, Kahfroushan D, 2020. Design and fabrication the novel polymeric magnetic boehmite nanocomposite (boehmite@ Fe<sub>3</sub>O<sub>4</sub>@PLA@SiO<sub>2</sub>) for the remarkable competitive adsorption of methylene blue and mercury ions. *Journal of Physics and Chemistry of Solids*, 144: 109515. <https://doi.org/10.1016/j.jpcs.2020.109515>
- Alorabi AQ, Azizi M, 2023. Effective removal of methyl green from aqueous environment using activated residual *Dodonaea Viscosa*: equilibrium, isotherm, and mechanism studies. *Environmental Pollutants and Bioavailability*, 35(1): 2168761. <https://doi.org/10.1080/26395940.2023.2168761>
- An CC, Zhang M, Xiao ZH, et al., 2023. Lignocellulose/chitosan hybrid aerogel composited with fluorescence molecular probe for simultaneous adsorption and detection of heavy metal pollutants. *Journal of Environmental Chemical Engineering*, 11(6): 111205. <https://doi.org/10.1016/j.jece.2023.111205>
- Angaru GKR, Lingamdinne LP, Choi YL, et al., 2021. Encapsulated zerovalent iron/nickel-fly ash zeolite foam for treating industrial wastewater contaminated by heavy metals. *Materials Today Chemistry*, 22: 100577. <https://doi.org/10.1016/j.mtchem.2021.100577>
- Aryee AA, Gao C, Han R, et al., 2022. Functionalized magnetic biocomposite based on peanut husk for the efficient sequestration of basic dyes in single and binary systems: Adsorption mechanism and antibacterial study. *Journal of Environmental Chemical Engineering*, 10(4): 108205. <https://doi.org/10.1016/j.jece.2022.108205>
- Azeez L, Adebisi SA, Adejumo AL, et al., 2022. Adsorptive properties of rod-shaped silver nanoparticles-functionalized biogenic hydroxyapatite for remediating methylene blue and congo red. *Inorganic Chemistry Communications*, 142: 109655. <https://doi.org/10.1016/j.inoche.2022.109655>
- Brahma D, Saikia H, 2022. Synthesis of ZrO<sub>2</sub>/MgAl-LDH composites and evaluation of its isotherm, kinetics and thermodynamic properties in the adsorption of congo red dye. *Chemical Thermodynamics and Thermal Analysis*, 7: 100067. <https://doi.org/10.1016/j.ctta.2022.100067>
- Cai L, 2018. Aniline degradation and dye decolorization with mixed bacteria in printing and dyeing wastewater. *China Dyeing and Finishing*, 44(17): 39-43.
- Cang JS, Li YJ, Liu DG, et al., 2021. Separation of trace Pb(II) and Cd(II) in dyeing wastewater by carbon dioxide driven ionic liquid two-phase extraction. *China Dyeing and Finishing*, 47(11): 67-70.
- Chanu HA, Onyari JM, Shiundu PM, 2019. Brewers' spent grain in adsorption of aqueous Congo Red and malachite Green dyes: Batch and continuous flow systems. *Journal of Hazardous Materials*, 380: 120897. <https://doi.org/10.1016/j.jhazmat.2019.120897>
- Chen L, Hu J, He YY, et al., 2024a. Microwave-assisted pyrolysis of waste lignin to prepare biochar for Cu<sup>2+</sup> highly-efficient adsorption: Performance, kinetics and mechanism resolution. *Separation and Purification Technology*, 342: 127070. <https://doi.org/10.1016/j.seppur.2024.127070>
- Chen RP, Gan CH, Cai BC, et al., 2024b. Co-adsorption and selective-adsorption of heavy metals and dyes from

- aqueous solution by bio-based humus/chitosan hydrogels. *Journal of Environmental Sciences*, 145: 193-204.  
<https://doi.org/10.1016/j.jes.2023.09.004>
- Debnath S, Das R, 2023. Strong adsorption of CV dye by Ni ferrite nanoparticles for waste water purification: Fits well the pseudo second order kinetic and Freundlich isotherm model. *Ceramics International*, 49(10): 16199-16215.  
<https://doi.org/10.1016/j.ceramint.2023.01.218>
- Du PY, Xu L, Ke ZJ, et al., 2022. A highly efficient biomass-based adsorbent fabricated by graft copolymerization: Kinetics, isotherms, mechanism and coadsorption investigations for cationic dye and heavy metal. *Journal of Colloid and Interface Science*, 616: 12-22.  
<https://doi.org/10.1016/j.jcis.2022.02.048>
- Fan C, Liang Y, Dong HQ, et al., 2018. Guanidinium ionic liquid-controlled synthesis of zeolitic imidazolate framework for improving its adsorption property. *Science of The Total Environment*, 640-641: 163-173.  
<https://doi.org/10.1016/j.scitotenv.2018.05.282>
- Ghafil AJ, Mazloom G, Abdi J, et al., 2024.  $Ti_3C_2T_x/ZIF-67$  hybrid nanocomposite as a highly effective adsorbent for Pb (II) removal from water: Synthesis and DFT calculations. *Applied Surface Science*, 643: 158642.  
<https://doi.org/10.1016/j.apsusc.2023.158642>
- Hajiahmadi Z, Moheb A, Mohammadi M, et al., 2024. Surface and mass transfer kinetic and equilibrium modeling of Pb(II) ions adsorption on hydroxyapatite scaffold: Batch and fixed-bed column studies. *Separation and Purification Technology*, 343: 127141.  
<https://doi.org/10.1016/j.seppur.2024.127141>
- Han RH, Zhang JJ, Pan H, et al., 2009. Study of equilibrium, kinetic and thermodynamic parameters about methylene blue adsorption onto natural zeolite. *Chemical Engineering Journal*, 145(3): 496-504.  
<https://doi.org/10.1016/j.cej.2008.05.003>
- He S, Sun JW, Jin X, et al., 2023. Adsorption enhancement of Congo red dye from wastewater based on edamame shell originated activated carbon by the cations: Experimental and theoretical studies. *Diamond and Related Materials*, 136: 109930.  
<https://doi.org/10.1016/j.diamond.2023.109930>
- Himanshu P, 2021. Review on Solvent Desorption Study from Exhausted Adsorbent. *Journal of Saudi Chemical Society*, 25(8): 101302.  
<https://doi.org/10.1016/j.jscs.2021.101302>
- Igberase E, Osifo P, Ofomaja A, 2018. Adsorption of metal ions by microwave assisted grafting of cross-linked chitosan beads. Equilibrium, isotherm, thermodynamic and desorption studies. *Applied Organometallic Chemistry*, 32(3): e4131.  
<https://doi.org/10.1002/aoc.4131>
- I.M.S. SF, A. A-GM, 2023. Waste-to-value: Synthesis of nano-aluminum oxide (nano- $\gamma$ - $Al_2O_3$ ) from waste aluminum foils for efficient adsorption of methylene blue dye. *Case Studies in Chemical and Environmental Engineering*, 8: 100394.  
<https://doi.org/10.1016/j.cscee.2023.100394>
- Jiang J, Huang XY, Bai JL, et al., 2022. Adsorption of clothianidin by potassium permanganate modified biochar in aqueous solution. *Journal of Environmental Engineering*, 16(04):1175-1185.
- Kalam S, A AS, Kamal MS, Shirish P, 2021. Surfactant Adsorption Isotherms: A Review. *ACS Omega*, 6(48): 32342-32348.  
<https://doi.org/10.1021/acsomega.1c04661>
- Kim SH, Chung H, Jeong S, et al., 2021. Identification of pH-dependent removal mechanisms of lead and arsenic by basic oxygen furnace slag: Relative contribution of precipitation and adsorption. *Journal of Cleaner Production*, 279: 123451.  
<https://doi.org/10.1016/j.jclepro.2020.123451>
- Kyzas GZ, Siafaka PI, Pavlidou EG, et al., 2015. Synthesis and adsorption application of succinyl-grafted chitosan for the simultaneous removal of zinc and cationic dye from binary hazardous mixtures. *Chemical Engineering Journal*, 259: 438-448.  
<https://doi.org/10.1016/j.cej.2014.08.019>
- Lan HC, Zhang S, Zhang JY, et al., 2023. Water-soluble carbon nitride as phase-convertible adsorbents for removing heavy metals from water. *Applied Surface Science*, 614: 156172.  
<https://doi.org/10.1016/j.apsusc.2022.156172>
- Li B, Guo JZ, Lv KL, et al., 2019c. Adsorption of methylene blue and Cd(II) onto maleylated modified hydrochar from water. *Environmental Pollution*, 254(PB): 113014.  
<https://doi.org/10.1016/j.envpol.2019.113014>
- Li B, Liu JL, Xu H, 2022. Synthesis of polyaminophosphonated-functionalized hydrochar for efficient sorption of Pb(II). *Environmental Science and Pollution Research*, 29: 49808-49815.  
<https://doi.org/10.1007/s11356-022-19350-4>
- Li B, Lv JQ, Guo JZ, et al., 2019a. The polyaminocarboxylated modified hydrochar for efficient capturing methylene blue and Cu(II) from water. *Bioresource Technology*, 275: 360-367.  
<https://doi.org/10.1016/j.biortech.2018.12.083>
- Li L, Bai YF, Qi CH, et al, 2024b. Adsorption of Pb(II) and Cu(II) by succinic anhydride-modified apple pomace. *Biochemical Engineering Journal*, 201: 109136.  
<https://doi.org/10.1016/j.bej.2023.109136>
- Li PP, Li Z, Liu SY, et al., 2024a. Imidazole/pyridine-based ionic liquids modified metal-organic frameworks for efficient adsorption of Congo red in water. *Journal of Molecular Structure*, 1303: 137599  
<https://doi.org/10.1016/j.molstruc.2024.137599>
- Li SH, Luo C, Yan F, et al., 2023. Remediation of Pb(II) and Cd(II) in polluted waters with calcium thioglycolate-modified straw biochar. *Environmental Pollution*, 338: 122638.  
<https://doi.org/10.1016/j.envpol.2023.122638>
- Li SQ, Fang ZL, Li Q, et al., 2019b. Magnetic metal-organic framework material and its application in printing and dyeing wastewater treatment (I). *China Dyeing and Finishing*, 45(22): 53-56.
- Liang YQ, Li H, Mao XM, et al., 2020. Competitive Adsorption of Methylene Blue and Cu(II) onto Magnetic Graphene Oxide/Alginate Beads. *Russian Journal of Physical Chemistry A*, 94(12): 2605-2613.  
<https://doi.org/10.1134/S0036024420120158>
- Lin JY, Ye WY, Xie M, et al., 2023. Environmental impacts and remediation of dye-containing wastewater. *Nature Reviews Earth & Environment*, 4:785-803.  
<https://doi.org/10.1038/s43017-023-00489-8>

- Liu B, Lv P, Wu RF, et al., 2023a. Coal gasification fine slag based multifunctional nanoporous silica microspheres for synergistic adsorption of Pb(II) and Congo red. *Separation and Purification Technology*, 323: 124478. <https://doi.org/10.1016/j.seppur.2023.124478>
- Liu FJ, He Q, Su L, et al., 2023b. Adsorption properties of methylene blue by surface functionalized magnetic biochar with sodium alginate. *Inorganic Chemicals Industry*, 56(02): 1-14. <https://doi.org/10.19964/j.issn.1006-4990.2023-0180>
- Liu S, Huang JH, Zhang W, et al., 2022b. Investigation of the adsorption behavior of Pb(II) onto natural-aged microplastics as affected by salt ions. *Journal of Hazardous Materials*, 431: 128643. <https://doi.org/10.1016/j.jhazmat.2022.128643>
- Liu Y, Qiu GY, Liu YF, et al., 2022a. Fabrication of CoFe-MOF materials by different methods and adsorption properties for Congo red. *Journal of Molecular Liquids*, 360: 119405. <https://doi.org/10.1016/j.molliq.2022.119405>
- Lu XY, Liao M, Xie XM, et al., 2024. The potential of biomass residue formed from microbial treatment of lacquer residue for adsorption and removal of dye from wastewater. *Acta Scientiae Circumstantiae*, 44(04): 82-94. <https://doi.org/10.13671/j.hjkxxb.2023.0373>
- Lv SW, Liu JM, Ma H, et al., 2019. Simultaneous adsorption of methyl orange and methylene blue from aqueous solution using amino functionalized Zr-based MOFs. *Microporous and Mesoporous Materials*, 282: 179-187. <https://doi.org/10.1016/j.micromeso.2019.03.017>
- Ma DS, Yi H, Lai C, et al., 2021. Critical review of advanced oxidation processes in organic wastewater treatment. *Chemosphere*, 275: 130104. <https://doi.org/10.1016/j.chemosphere.2021.130104>
- Meneses IP, Novaes SD, Dezotti RS, et al., 2022. CTAB-modified carboxymethyl cellulose/bagasse cryogels for the efficient removal of bisphenol A, methylene blue and Cr(VI) ions: Batch and column adsorption studies. *Journal of Hazardous Materials*, 421: 126804-126804. <https://doi.org/10.1016/j.jhazmat.2021.126804>
- Mondal MIH, Chakraborty SC, Rahman MS, et al., 2024. Adsorbents from rice husk and shrimp shell for effective removal of heavy metals and reactive dyes in water. *Environmental Pollution*, 346: 123637. <https://doi.org/10.1016/j.envpol.2024.123637>
- Morteza C, Reza NM, Arash A, Morteza T, et al., 2021. Removal of Ni and Zn heavy metal ions from industrial waste waters using modified slag of electric arc furnace. *Materials Research Express*, 8(5). <https://doi.org/10.1088/2053-1591/abf520>
- Mu ZH, Liu DN, Lv J, et al., 2022. Insight into the highly efficient adsorption towards cationic methylene blue dye with a superabsorbent polymer modified by esterified starch. *Journal of Environmental Chemical Engineering*, 10(5): 108425. <https://doi.org/10.1016/j.jece.2022.108425>
- Nitish S, Divya M, Manjunath C, et al., 2023. Adsorptive removal of Congo Red dye from its aqueous solution by Ag-Cu-CeO<sub>2</sub> nanocomposites: Adsorption kinetics, isotherms, and thermodynamics. *Heliyon*, 9(11): e22027. <https://doi.org/10.1016/j.heliyon.2023.e22027>
- Nizam T, Krishnan KA, Joseph A, et al., 2024. Isotherm, kinetic and thermodynamic modelling of liquid phase adsorption of the heavy metal ions Zn(II), Pb(II) and Cr(VI) onto MgFe<sub>2</sub>O<sub>4</sub> nanoparticles. *Groundwater for Sustainable Development*, 25: 101120. <https://doi.org/10.1016/j.gsd.2024.101120>
- Qin XM, Bai L, Tan YZ, et al., 2019.  $\beta$ -Cyclodextrin-crosslinked polymeric adsorbent for simultaneous removal and stepwise recovery of organic dyes and heavy metal ions: Fabrication, performance and mechanisms. *Chemical Engineering Journal*, 372: 1007-1018. <https://doi.org/10.1016/j.cej.2019.05.006>
- Selim QA, Mohamed AE, Mobarak M, et al., 2018. Cr(VI) uptake by a composite of processed diatomite with MCM-41: Isotherm, kinetic and thermodynamic studies. *Microporous and Mesoporous Materials*, 260: 84-92. <https://doi.org/10.1016/j.micromeso.2017.10.041>
- Sepideh K, Ahmad KS, Samaneh M, 2024. Use of NIR/NaBH<sub>4</sub> combinatorial techniques for simultaneous and high-efficient adsorption of heavy metal ions from contaminated water by Chitosan/Au Janus microdisks. *Surfaces and Interfaces*, 44: 103801. <https://doi.org/10.1016/j.surfin.2023.103801>
- Shubham S, Jyoti J, 2024. A comparative assessment of the methylene blue dye adsorption capacity of natural biochar versus chemically altered activated carbons. *Bioresource Technology Reports*, 25: 01726. <https://doi.org/10.1016/j.biteb.2023.101726>
- Song YL, Wang LJ, Qiang X, et al., 2023. An overview of biological mechanisms and strategies for treating wastewater from printing and dyeing processes. *Journal of Water Process Engineering*, 55: 104242. <https://doi.org/10.1016/j.jwpe.2023.104242>
- Sumanta S, Nisarani S, Kumar SM, et al., 2021. Investigating the selectivity and interference behavior for detoxification of Cr(VI) using lanthanum phosphate polyaniline nanocomposite via adsorption-reduction mechanism. *Chemosphere*, 278: 130507. <https://doi.org/10.1016/j.chemosphere.2021.130507>
- Tang J, Zhang YF, Liu Y, et al., 2020. Efficient ion-enhanced adsorption of congo red on polyacrolein from aqueous solution: Experiments, characterization and mechanism studies. *Separation and Purification Technology*, 252: 117445. <https://doi.org/10.1016/j.seppur.2020.117445>
- Tattibayeva Z, Tazhibayeva S, Kujawski W, et al., 2022. Peculiarities of adsorption of Cr (VI) ions on the surface of *Chlorella vulgaris* ZBS1 algae cells. *Heliyon*, 8:e10468. <https://doi.org/10.1016/j.heliyon.2022.e10468>
- Tran CC, Dong HC, Truong VTN, et al., 2022. Enhancing the remarkable adsorption of Pb<sup>2+</sup> in a series of sulfonic-functionalized Zr-based MOFs: a combined theoretical and experimental study for elucidating the adsorption mechanism. *Dalton transactions (Cambridge, England : 2003)*, 51(19): 7503-7516. <https://doi.org/10.1039/d2dt01009g>
- Vikram GS, V.V. K, Md. A, 2024. Fabrication of a bio-adsorbent material by grafting CeO<sub>2</sub> quantum dots (QDs) over Areca nut shell biochar using Saccharum officinarum extract as a solvent/capping agent for adsorption of Methylene blue dye: Synthesis, material

- analyses, adsorption kinetics and isotherms studies. *Colloids and Surfaces A: Physicochemical and Engineering Aspects*, 680: 132611.  
<https://doi.org/10.1016/j.colsurfa.2023.132611>
- Visa M, Bogatu C, Duta A, 2010. Simultaneous adsorption of dyes and heavy metals from multicomponent solutions using fly ash. *Applied Surface Science: A Journal Devoted to the Properties of Interfaces in Relation to the Synthesis and Behaviour of Materials*, 256(17): 5486-5486.  
<https://doi.org/10.1016/j.apsusc.2009.12.145>
- Wang D, Chen HS, Xin CY, et al., 2024b. Insight into adsorption of Pb(II) with wild resistant bacteria TJ6 immobilized on biochar composite: Roles of bacterial cell and biochar. *Separation and Purification Technology*, 331: 125660.  
<https://doi.org/10.1016/j.seppur.2023.125660>
- Wang J, Gao ML, Shen T, et al., 2019. Insights into the efficient adsorption of rhodamine B on tunable organo-vermiculites. *Journal of Hazardous Materials*, 366: 501-511.  
<https://doi.org/10.1016/j.jhazmat.2018.12.031>
- Wang SB, Ariyanto E, 2007. Competitive adsorption of malachite green and Pb ions on natural zeolite. *Journal of Colloid and Interface Science*, 314(1): 25-31.  
<https://doi.org/10.1016/j.jcis.2007.05.032>
- Wang T, Liu W, Xiong L, et al., 2013. Influence of pH, ionic strength and humic acid on competitive adsorption of Pb(II), Cd(II) and Cr(III) onto titanate nanotubes. *Chemical Engineering Journal*, 215: 366-374.  
<https://doi.org/10.1016/j.cej.2012.11.029>
- Wang Y, Yu S, Yuan HW, et al., 2024a. Constructing N, S co-doped network biochar confined CoFe<sub>2</sub>O<sub>4</sub> magnetic nanoparticles adsorbent: Insights into the synergistic and competitive adsorption of Pb<sup>2+</sup> and ciprofloxacin. *Environmental Pollution*, 343: 123178.  
<https://doi.org/10.1016/j.envpol.2023.123178>
- Wu SJ, Li MY, Xin LL, et al., 2022. Efficient removal of Cr(VI) by triethylenetetramine modified sodium alginate/carbonized chitosan composite via adsorption and photocatalytic reduction. *Journal of Molecular Liquids*, 366:120160.  
<https://doi.org/10.1016/j.molliq.2022.120160>
- Wu ZD, Wang XM, Yao J, et al., 2021. Synthesis of polyethyleneimine modified CoFe<sub>2</sub>O<sub>4</sub>-loaded porous biochar for selective adsorption properties towards dyes and exploration of interaction mechanisms. *Separation and Purification Technology*, 277: 119474.  
<https://doi.org/10.1016/j.seppur.2021.119474>
- Xie WJ, Pakdel E, Liang YJ, et al., 2020. Natural melanin/TiO<sub>2</sub> hybrids for simultaneous removal of dyes and heavy metal ions under visible light. *Journal Of Photochemistry And Photobiology A-chemistry*, 389: 112292.  
<https://doi.org/10.1016/j.jphotochem.2019.112292>
- Yang W, Kong YD, Yin H, et al., 2023. Study on the adsorption performance of ZIF-8 on heavy metal ions in water and the recycling of waste ZIF-8 in cement. *Journal of Solid State Chemistry*, 326:124217.  
<https://doi.org/10.1016/j.jssc.2023.124217>
- Ye WY, Liu RR, Chen XY, et al., 2020b. Loose nanofiltration-based electrodialysis for highly efficient textile wastewater treatment. *Journal of Membrane Science*, 608:118182.  
<https://doi.org/10.1016/j.memsci.2020.118182>
- Ye WY, Ye KF, Lin F, et al., 2020a. Enhanced fractionation of dye/salt mixtures by tight ultrafiltration membranes via fast bio-inspired co-deposition for sustainable textile wastewater management. *Chemical Engineering Journal*, 379:122321.  
<https://doi.org/10.1016/j.cej.2019.122321>
- Ye WY, Yu F, Yu ZJ, et al., 2024. High-performance anti-bacterial tight ultrafiltration membrane constructed by co-deposition of dopamine and tobramycin for sustainable high-salinity textile wastewater management. *Desalination*, 579:117482.  
<https://doi.org/10.1016/j.desal.2024.117482>
- Zhang QY, Wang X, Chen HB, et al., 2023a. Eco-friendly and magnetic sucrose-derived Fe-containing mesoporous carbon composites for high-efficiency Congo red adsorption and supercapacitor applications. *Diamond and Related Materials*, 139: 110268.  
<https://doi.org/10.1016/j.diamond.2023.110268>
- Zhang YB, Zhang L, Wang NN, et al., 2023b. Citric acid modified  $\beta$ -cyclodextrin for the synthesis of water-stable and recoverable CD-MOF with enhanced adsorption sites: Efficient removal of Congo red and copper ions from wastewater. *Journal of Environmental Chemical Engineering*, 11(6): 111413.  
<https://doi.org/10.1016/j.jece.2023.111413>

## Electronic supplementary materials

Appendix A, Table S1-S2, Figs. S1-S10

## 中文概要

**题目:** 漆渣经微生物处理形成的生物质渣对同步吸附去除废水中重金属和染料的研究

**作者:** 陆欣悦<sup>1</sup>, 廖敏<sup>1</sup>, 谢晓梅<sup>2</sup>, 邱浩<sup>1</sup>, 袁枫<sup>1</sup>, 罗哲<sup>1</sup>, 樊春林<sup>3</sup>

**机构:** <sup>1</sup>浙江大学, 环境与资源学院, 浙江省农业资源与环境重点实验室, 中国杭州, 310058; <sup>2</sup>环境与资源国家级实验教学示范中心(浙江大学), 中国杭州, 310058; <sup>3</sup>宁波费尔诺生物科技有限公司, 中国宁波, 315502

**目的:** 本文旨在探究 LBM 对 Pb<sup>2+</sup>和染料 MB 或 CR 两者的同步去除能力以及之间存在的竞争吸附行为, 从而揭示其应用潜力, 以期对印染废水中重金属和染料复合污染的同步处理提供一种廉价易得且绿色环保的生物质材料, 实现以废治废的目标和废弃物资源化利用的可能。

**创新点:** 1. 发现 LBM 可作为同步去除重金属和染料复合污染 (Pb<sup>2+</sup>-MB/CR) 的新型吸附材料; 2. 揭示氢键作用、络合作用、 $\pi$ - $\pi$  键相互作用和静电作用

等是 LBM 与  $\text{Pb}^{2+}$  和染料 MB 或 CR 间的主要作用机制。

**方法:** 1. 通过单因素实验分析, 探究 LBM 同步吸附去除  $\text{Pb}^{2+}$ -MB/CR 复合体系的能力及其影响作用, 并分析其吸附动力学、等温吸附及吸附热力学特征; 2. 以吸收能力之比  $R_{q,i}$  (式 9) 对  $\text{Pb}^{2+}$  和 MB 或 CR 之间的相互作用进行评估。并以常见的共存阴阳离子为例探究其对  $\text{Pb}^{2+}$ -MB/CR 复合体系吸附的作用; 3. 对复合体系的吸附态分别采用了三种不同解吸剂进行解吸, 了解 LBM 吸附态的稳定性及 LBM 在吸附后的再生循环利用潜力; 4. 通过扫描电子显微镜(SEM)、X 射线衍射(XRD) 及傅里叶红外光谱 (FTIR) 表征其吸附行为。

**结论:** 1. 准二级动力学模型 ( $R^2 > 0.99$ ) 可以描述  $\text{Pb}^{2+}$ -MB/CR 复合体系的吸附动力学。在两种体系中, 在一定范围内适当增加 LBM 的投加量和体系温度有利于  $\text{Pb}^{2+}$ -MB/CR 复合体系的吸附。最佳固液比和温度分别为 1:75 和  $30^\circ\text{C}$ , 对  $\text{Pb}^{2+}$  和 MB 的吸附去除率随着 pH 的升高而升高, 随着溶液中离子强度的增加而减少, 而对 CR 的去除率则相反; 2. 在  $\text{Pb}^{2+}$ -MB 复合体系中, 吸附呈拮抗关系。而在  $\text{Pb}^{2+}$ -CR 复合体系中, 两者存在协同吸附过程。上述两种体系中, 共存阴阳离子对同步吸附去除  $\text{Pb}^{2+}$ 、MB 和 CR 的影响有限; 3. 解吸结果表明, LBM 可作为一次性材料同时处理  $\text{Pb}^{2+}$ -MB/CR 复合体系; 4. LBM 的结构、各种无机和有机成分对  $\text{Pb}^{2+}$ -MB/CR 复合体系的同步吸附做出贡献, 表征结果显示两种复合体系的吸附主要受氢键作用、络合作用、 $\pi$ - $\pi$  键相互作用和静电作用等共同控制。

**关键词:** 漆渣生物质; 铅; 亚甲基蓝; 刚果红; 同步吸附去除